Report

Cell Reports

Transforming Growth Factor-β3 Regulates Adipocyte Number in Subcutaneous White Adipose Tissue

Graphical Abstract

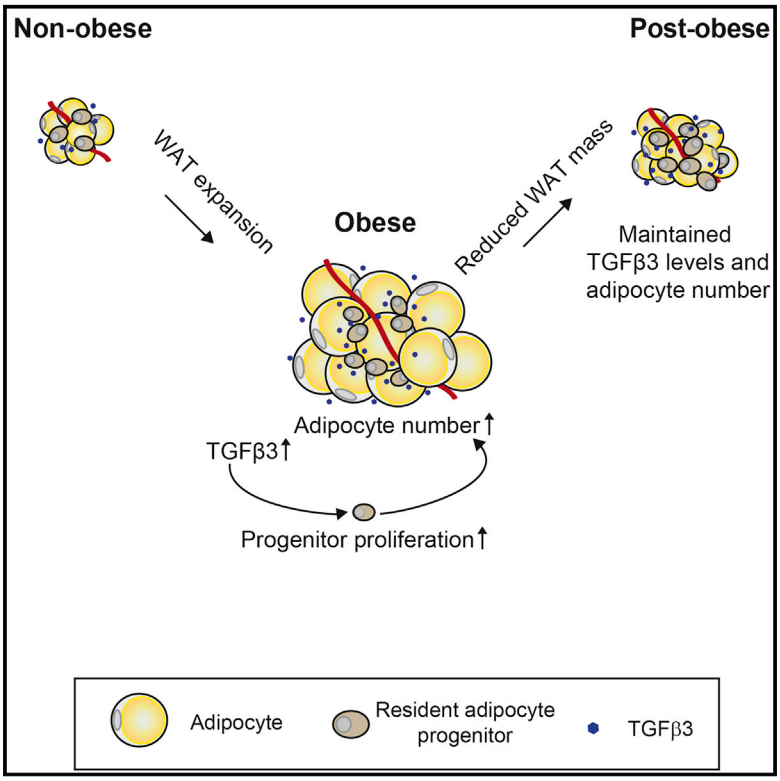

Highlights

- Increases in adipose mass lead to an irreversible increase in adipocyte number
- Adipocyte number is linked to the adipose expression of a set of growth factors
- Among these, only TGFβ3 stimulates adipocyte progenitor proliferation
- *Tgfb3*$^{+/-}$ mice display adipose hypertrophy and glucose intolerance upon weight gain

Authors

Paul Petrus, Niklas Mejhert, Patricia Corrales, ..., Gema Medina-Gomez, Peter Arner, Mikael Rydén

Correspondence

gema.medina@urjc.es (G.M.-G.), mikael.ryden@ki.se (M.R.)

In Brief

The mechanisms regulating adipocyte number upon increases in white adipose tissue mass are not known. Here, by combining prospective clinical studies with cell and animal models, Petrus et al. report that transforming growth factor-β3 increases adipocyte precursor proliferation and thereby enables hyperplastic white adipose tissue expandability.

Petrus et al., 2018, Cell Reports *25*, 551–560
October 16, 2018
https://doi.org/10.1016/j.celrep.2018.09.069

CellPress

Cell Reports
Report

Transforming Growth Factor-β3 Regulates Adipocyte Number in Subcutaneous White Adipose Tissue

Paul Petrus,[1,7] Niklas Mejhert,[1,7] Patricia Corrales,[2] Simon Lecoutre,[1] Qian Li,[1] Estela Maldonado,[3] Agne Kulyté,[1] Yamila Lopez,[2] Mark Campbell,[4] Juan R. Acosta,[1] Jurga Laurencikiene,[1] Iyadh Douagi,[1] Hui Gao,[5] Concepción Martínez-Álvarez,[3] Per Hedén,[6] Kirsty L. Spalding,[1] Antonio Vidal-Puig,[4] Gema Medina-Gomez,[2,*] Peter Arner,[1] and Mikael Rydén[1,8,*]

[1]Department of Medicine (H7), Karolinska Institutet, Stockholm 141 86, Sweden
[2]Departamento de Ciencias Básicas de la Salud, Área Bioquímica y Biología Molecular, Facultad de Ciencias de la Salud, Universidad Rey Juan Carlos, Alcorcón 289 22, Madrid, Spain
[3]Departamento de Anatomía y Embriología, Facultad de Medicina, Facultad de Odontología, Universidad Complutense, Madrid 28040, Spain
[4]MRC MDU, Metabolic Research Laboratories, Institute of Metabolic Science, Box 289, Addenbrooke's Hospital, Cambridge CB2 0QQ, UK
[5]Department of Biosciences and Nutrition, Karolinska Institutet, Stockholm 141 86, Sweden
[6]Akademikliniken, Storängsvägen 10, Stockholm 115 42, Sweden
[7]These authors contributed equally
[8]Lead Contact
*Correspondence: gema.medina@urjc.es (G.M.-G.), mikael.ryden@ki.se (M.R.)
https://doi.org/10.1016/j.celrep.2018.09.069

SUMMARY

White adipose tissue (WAT) mass is determined by adipocyte size and number. While adipocytes are continuously turned over, the mechanisms controlling fat cell number in WAT upon weight changes are unclear. Herein, prospective studies of human subcutaneous WAT demonstrate that weight gain increases both adipocyte size and number, but the latter remains unaltered after weight loss. Transcriptome analyses associate changes in adipocyte number with the expression of 79 genes. This gene set is enriched for growth factors, out of which one, transforming growth factor-β3 (TGFβ3), stimulates adipocyte progenitor proliferation, resulting in a higher number of cells undergoing differentiation *in vitro*. The relevance of these observations was corroborated *in vivo* where *Tgfb3*$^{+/-}$ mice, in comparison with wild-type littermates, display lower subcutaneous adipocyte progenitor proliferation, WAT hypertrophy, and glucose intolerance. TGFβ3 is therefore a regulator of subcutaneous adipocyte number and may link WAT morphology to glucose metabolism.

INTRODUCTION

White adipose tissue (WAT) mass is determined by its cellularity—in other words, the size and number of adipocytes. Cross-sectional analyses in adult human WAT have shown that both measures are markedly higher in obesity, albeit to a variable degree (Hirsch and Batchelor, 1976). The relation between fat mass and fat cell size is modeled by an asymptotic curve (Spalding et al., 2008), which reflects the fact that human adipocytes can only attain a maximum volume of ~2,000 pL. This has resulted in the hypothesis that WAT expansion depends on both increased fat cell size (hypertrophy) and number (hyperplasia) (Hirsch and Batchelor, 1976; Spalding et al., 2008), processes that may be of pathophysiological relevance. Thus, while WAT hypertrophy is associated with insulin resistance and increased risk of type 2 diabetes, hyperplasia is protective (Arner et al., 2011; Weyer et al., 2000) and is dependent on the proliferation and differentiation of adipocyte precursors present in the stromal-vascular fraction (SVF) of WAT. However, the relative contribution of either expansion mode under hypercaloric conditions has been debated. An older overfeeding study, which resulted in a 21% body weight increase in 6 months, concluded that WAT grew primarily via hypertrophy (Salans et al., 1971). In contrast, data from an 8-week-long study (7% increase in body weight) in normal-weight individuals suggested that abdominal subcutaneous WAT (sWAT) expanded primarily via hypertrophy, while femoral sWAT increased via hyperplasia (Tchoukalova et al., 2010). Other reports have not been able to detect changes in fat cell size (Alligier et al., 2012; Samocha-Bonet et al., 2010) or number (Alligier et al., 2012), but these interventions resulted only in modest body weight increases (3%–4%) and were relatively short (28–56 days). Because the annual turnover of adipocytes in adult humans is ~10% (Spalding et al., 2008), it is possible that short-term interventions may not result in detectable changes in WAT cellularity. In a long-term study, we recently demonstrated that subcutaneous abdominal fat cell number increased in obese subjects who regained weight between 2 and 5 years after bariatric surgery (Hoffstedt et al., 2017). This resulted in hyperplastic sWAT and a healthier metabolic phenotype compared with body weight-matched never-obese controls. Human sWAT may expand via both hypertrophy and hyperplasia, and the relative contribution of either mechanism can be of relevance in relation to metabolic phenotype.

Subcutaneous adipocyte number increases during adolescence, plateaus in early adulthood among weight-stable

individuals (Spalding et al., 2008), and is doubled in obese subjects compared with non-obese individuals (Spalding et al., 2008). However, WAT mass loss, whether voluntary (Spalding et al., 2008) or involuntary (Rydén et al., 2008), significantly reduces adipocyte volume, whereas fat cell number remains unaltered. From this follows that obese subjects who have attained a non-obese state (termed "post-obese") display WAT hyperplasia in comparison with weight-matched never-obese individuals (Löfgren et al., 2005). Thus, increases in WAT mass appear to generate a new set point for adipocyte number that remains unaltered by long-term weight loss and may be protective against metabolic complications upon weight regain (Hoffstedt et al., 2017). This suggests that specific mechanisms operate within WAT to increase fat cell production during weight gain and maintain elevated adipocyte numbers in adults after weight reduction. Nevertheless, the endogenous factors controlling fat cell number have remained unknown.

Morphometric results in human WAT can be compared with data obtained in animal models. Thus, using different cell-tracking techniques, studies in male mice have demonstrated that diet-induced obesity stimulates both hypertrophic and hyperplastic expansion of epididymal WAT (often defined as "visceral" [vWAT]), while inguinal WAT (often defined as "subcutaneous," sWAT) only grows via hypertrophy (Jeffery et al., 2015; Wang et al., 2013b). This notion was recently made more complex by findings demonstrating that sWAT of female mice display both hypertrophic and hyperplastic expansion (Jeffery et al., 2016). In the same study, these gender-related differences were shown to depend on the microenvironment and not on intrinsic differences between adipocyte precursors. All of this suggests that murine WAT displays depot- and gender-specific differences in expansion upon diet-induced obesity. While there may be qualitative differences in these processes between mice and humans, it is still valid to determine the impact of specific genes in murine models.

To identify regulators controlling fat cell number upon changes in WAT mass, we adopted a translational approach by combining clinical prospective studies with experimental models. This resulted in the identification of transforming growth factor-β3 (TGFβ3), a secreted protein expressed in the SVF of sWAT, which stimulates adipocyte precursor proliferation and regulates fat cell number *in vitro* and *in vivo*.

RESULTS

The Relation between Body Weight Changes and WAT Cellularity

To monitor cellularity alterations over time, we studied two cohorts of women from whom repeated abdominal sWAT biopsies were obtained. Cohort 1 (Table S1) consisted of 27 women from a previous study examining the long-term effects of weight changes (mean follow-up of 10 years) (Andersson et al., 2009). Anthropometric measures, total WAT mass, and mean fat cell size and number were determined at baseline and follow-up. The group was divided into tertiles based on spontaneous changes in body weight over time. In contrast to weight-stable subjects, individuals who markedly gained weight (on average 18%, range 9%–27%) displayed a significant increase in body fat mass, subcutaneous fat cell volume, and total adipocyte number (Figures 1A–1C). Changes in sWAT cellularity following pronounced weight loss were determined in a second group of individuals (cohort 2; Table S2), which consisted of 21 severely obese women who had reached a non-obese (i.e., post-obese) state (BMI <30 kg/m^2) 2 years after bariatric surgery. Results were compared with samples obtained from age-, BMI-, and body fat mass-matched control women who had never been obese (cohort 3, detailed together with cohort 2 in Table S2). The number of subcutaneous adipocytes in the post-obese subjects was unaltered despite pronounced WAT mass loss and therefore significantly higher than that in never-obese controls (Figures 1D–1F).

To address whether weight gain achieved during different periods of life could affect WAT cellularity, the 21 obese women in cohort 2 were subdivided according to whether they had been overweight (BMI ≥25 kg/m^2) before (n = 11) or after (n = 10) 18 years of age. Total WAT and subcutaneous adipocyte size and number were similar between the two groups, both before and after weight loss, suggesting that early or late onset of excess weight gain does not affect any of the studied parameters (Table S2).

Genes Linked to Subcutaneous Fat Cell Number Are Enriched for Growth Factors

Weight gain induces significant alterations in the expression of WAT genes involved in, for example, inflammation, extracellular matrix formation, lipid metabolism, and insulin signaling. Virtually all of these pathways are normalized upon weight loss (Rosen and Spiegelman, 2014). To identify factors potentially regulating adipocyte number, we reasoned that the corresponding gene subset would fulfill the following criteria: (1) altered in obesity, (2) unaltered by weight loss, and (3) significantly different between the post-obese and never-obese state, thereby mirroring the differences in fat cell number in these conditions. Microarray analyses of sWAT from cohorts 2 and 3 confirmed that the global transcriptional profile in obesity was normalized by weight loss (Figure 1G; Table S3) and was overrepresented by pathways belonging to inflammation, extracellular matrix components, and lipid metabolism (Table S4). However, 91 probe sets (Figure 1H), corresponding to 79 unique genes, were altered in obesity and remained dysregulated in the post-obese state (i.e., not normalized by weight loss). Pathway analyses revealed an overrepresentation of genes encoding proteins present in the extracellular compartment as well as growth factors (GFs), including *TGFB3*, chemokine (C-X-C motif) ligand 12 (*CXCL12*), fibroblast GF 7 (*FGF7*), osteoglycin (*OGN*), and platelet-derived GF D (*PDGFD*) (Figure 1I). To determine whether any of the 79 genes were affected by short-term weight gain, their expression in sWAT was extracted from a previously published study (Alligier et al., 2012). This retrospective analysis identified 12 genes to be significantly altered by overfeeding, four of which (*TGFB3*, *CXCL12*, *OGN*, and *PDGFD)* were among the GFs identified in the present study.

TGFβ3 Stimulates Adipocyte Precursor Proliferation and Fat Cell Number *In Vitro*

Fat cells are continuously generated from proliferating precursor cells in the SVFs of WAT. Because our analyses demonstrated

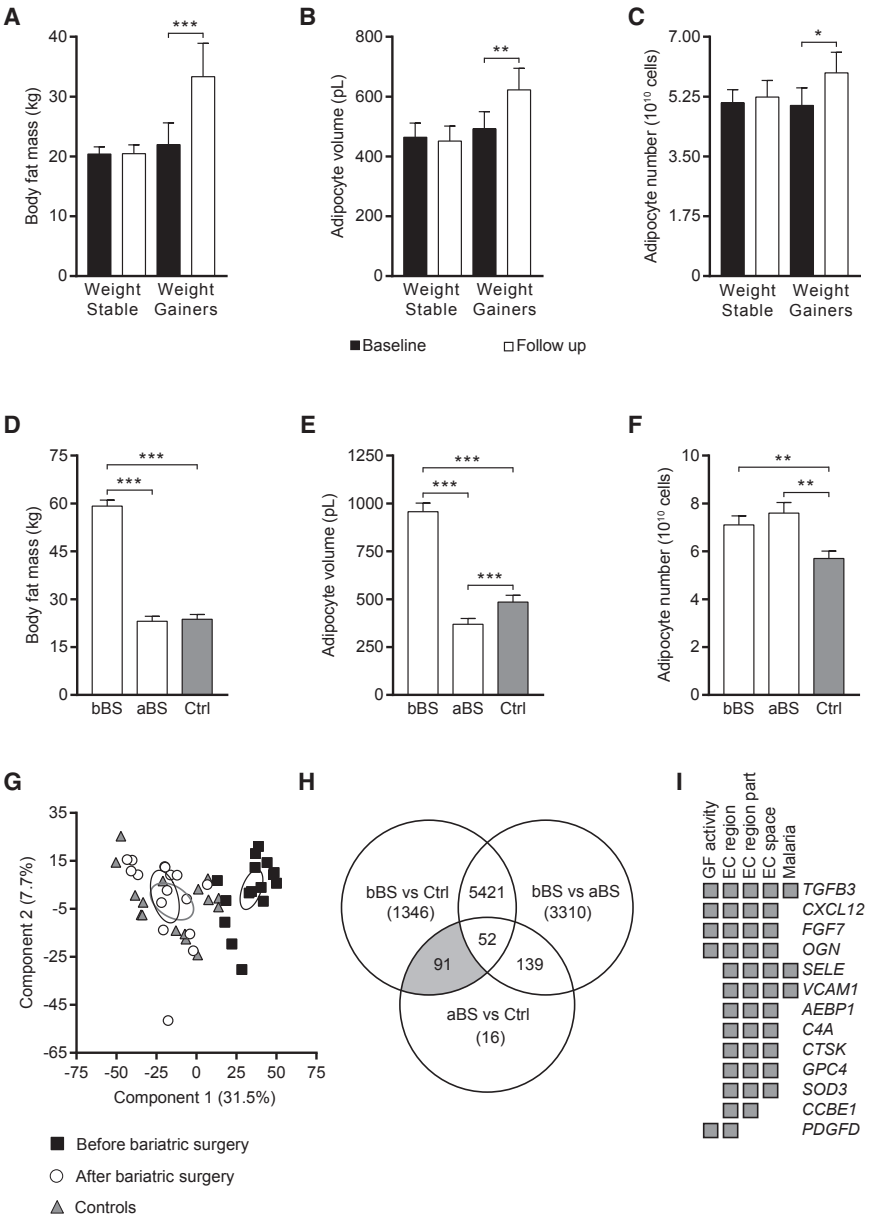

Figure 1. Effects of Weight Alterations on White Adipose Tissue Cellularity and Gene Expression

(A–C) Subjects in cohort 1 were subdivided into weight stable and weight gainers. Differences in body fat mass (A), adipocyte volume (B), and number (C) are shown. Black bars are at baseline and white bars are at 10-year follow-up.

(D–F) The same parameters (body fat mass in D, adipocyte volume in E, and adipocyte number in F) are displayed for cohorts 2 and 3 comprising obese subjects before and after bariatric surgery (bBS and aBS, respectively, white bars) and never-obese matched controls (Ctrl, gray bars).

(G) Principal-component analysis based on highly expressed transcripts in subcutaneous abdominal white adipose tissue from cohorts 2 and 3. Groups are separated with 95% confidence intervals if the circles are not overlapping each other. The contribution of each principal component is indicated as a percentage.

(H) Venn diagram displaying significantly altered probe sets comparing obese before bariatric surgery with never-obese controls (bBS versus Ctrl), obese before and after bariatric surgery (bBS versus aBS), and post-obese with never-obese controls (aBS versus Ctrl).

(I) Enriched pathways among the 91 probe sets (corresponding to 79 unique genes) altered in obesity, not normalized by weight loss, and still perturbed in the post-obese state. Only the genes present in at least two pathways are displayed.

Student's t tests were used to evaluate the results, and statistical differences are indicated as *$p < 0.05$, **$p < 0.01$, and ***$p < 0.001$. Error bars in (A)–(F) are SEM.

that specific GFs were increased upon short-term weight gain and were overrepresented among genes linked to fat cell number in post-obese subjects, further studies were focused on these factors. Analyses of mRNA expression in intact or fractionated human sWAT revealed that the corresponding GF genes were primarily expressed in the SVF and only to a limited degree in mature adipocytes (Figure S1A). Furthermore, microarray data from fractionated SVFs (Acosta et al., 2017) showed that all GFs were primarily expressed in the adipocyte progenitor ($CD45^-$/$CD34^+$/$CD31^-$) cell fraction (graphs not shown). These findings were confirmed at the protein level for four of the factors. CXCL12, FGF7, OGN, and TGFβ3 were secreted by undifferentiated human subcutaneous adipocyte precursor cells *in vitro*, and the levels were reduced during adipogenesis (Figure S1B).

PDGFD was excluded from further studies because it could not be detected using various commercial ELISA kits. The proliferative effect of each recombinant protein was assessed in human adipose-derived stem cells (hASCs). This revealed that only one, TGFβ3, stimulated proliferation (measured as cell density by 3-[4,5-dimethylthiazol-2-yl]-2,5 diphenyltetrazolium bromide [MTT] assay) in a concentration-dependent manner (Figure 2A). Similar results were observed in 3T3-L1 cells and primary murine adipose SVF cells (graphs not shown). In proliferating hASCs, *TGFB3* knock down by RNAi resulted in a marked downregulation of its mRNA expression (Figure 2B). This caused attenuated cell proliferation, which could be rescued by incubation with increasing concentrations of recombinant TGFβ3 (Figure 2C). The link between TGFβ3 and fat cell number was further substantiated by the observation that incubation with recombinant TGFβ3 followed by induction of adipocyte differentiation resulted in a significant increase in the formation of adipocytes (Figures 2D and 2E). This was achieved without affecting adipogenesis per se, as the expression of classical white adipocyte markers (*ADIPOQ*, *PPARG*, and *PLIN1*) was not affected in

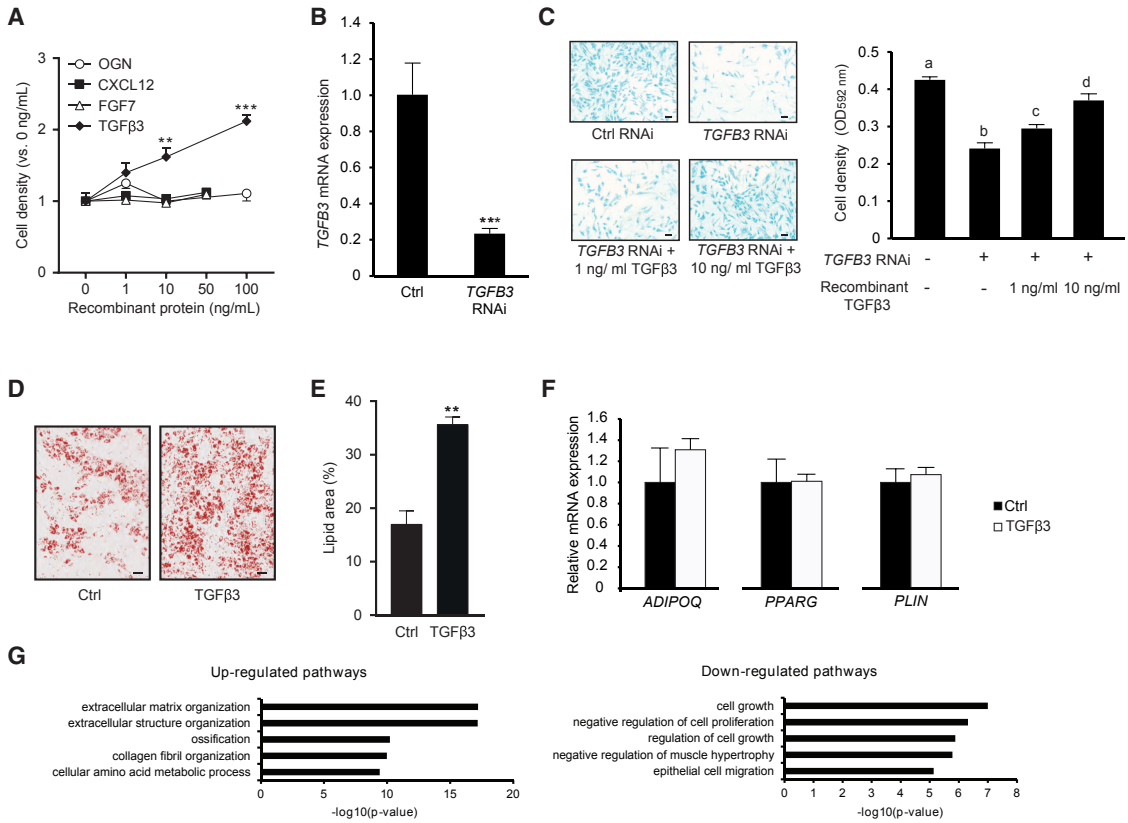

Figure 2. Effects of TGFβ3 in Human Adipocytes *In Vitro*

(A) Proliferative effects of recombinant CXCL12 (1–50 ng/mL), OGN (1–100 ng/mL), FGF7 (1–50 ng/mL), or TGFβ3 (1–100 ng/mL) in *in vitro* cultured human adipose-derived stem cells (hASCs). Cell density was determined by MTT as described in the STAR Methods and expressed as fold change versus cells incubated in control medium.

(B and C) hASCs were transfected with *TGFB3* or non-silencing small interfering RNA (siRNA) oligonucleotides. This resulted in a significant knock down of *TGFB3* mRNA expression (B). It also induced a significant attenuation of cell density or number determined by MTT, an effect that was rescued in a concentration-dependent manner by recombinant TGFβ3 protein (C).

(D and E) hASCs were first incubated with 10 ng/mL recombinant TGFβ3 for 72 hr. After removal of TGFβ3 for an additional 72 hr, adipogenesis was induced as described in the STAR Methods. Triglyceride accumulation at terminal differentiation was determined by oil red O staining (D) and quantified using ImageJ (E).

(F) Effects on adipocyte-specific gene expression were determined by qPCR in differentiated cells treated as in (D).

(G) hASCs were incubated with 10 ng/mL TGFβ3 for 24 hr. Cells were lysed and RNA analyzed by gene microarray. Bioinformatic analysis identified the top five upregulated and downregulated pathways, respectively.

In (A), (B), and (E), Student's t test was used to evaluate the results, and statistical differences are indicated as $^{**}p < 0.01$ and $^{***}p < 0.001$. In (C), ANOVA and post hoc tests were used to evaluate the results, and statistically significant differences ($p < 0.05$) between conditions are indicated by connecting letters. Scale bars, 100 μm. Error bars in (A) are SEM, and in (B), (C), and (E)–(F), error bars are SD.

TGFβ3-incubated compared with control-incubated cells (Figure 2F). To gain insights into the pathways induced by TGFβ3, hASCs were incubated for 24 hr with recombinant protein. In concordance with the observed *in vitro* effects, array analyses showed that the most significantly downregulated genes were involved in cell growth and negative regulation of cell proliferation, while the upregulated ones were involved in extracellular matrix organization (Figures 2G and S1C).

Unique Regulation of TGFβ3 Expression in Relation to Other TGFβ Members in sWAT

TGFβ3 belongs to a family of GFs that currently comprises three members in mammals (TGFβ1to -3). Although all three genes (*TGFB1* to *-3*) display large sequence homologies in their active domains, the individual proteins play distinct roles, as evidenced both by their activation of specific cell-surface receptors and the phenotypes of isoform-specific knockout mice (Laverty et al., 2009). Analyses of microarray data in cohorts 2 and 3 revealed that the expression of both *TGFB1* and *TGFB3* were higher in obesity, but that *TGFB1*, in contrast to *TGFB3*, was normalized in the post-obese state; in contrast *TGFB2* was not affected by either obesity or weight loss (Figure S1D). The expression patterns of *TGFB1* to *-3* in cohorts 2 and 3 were validated by qPCR (Figure S1E). We somewhat unexpectedly found that the levels of *TGFB3* in vWAT were lower in obese compared with non-obese subjects (Figure S1F). This suggests that the link between increased TGFβ3 levels and adipocyte number in obesity is specific for this TGFβ member and only for the subcutaneous depot.

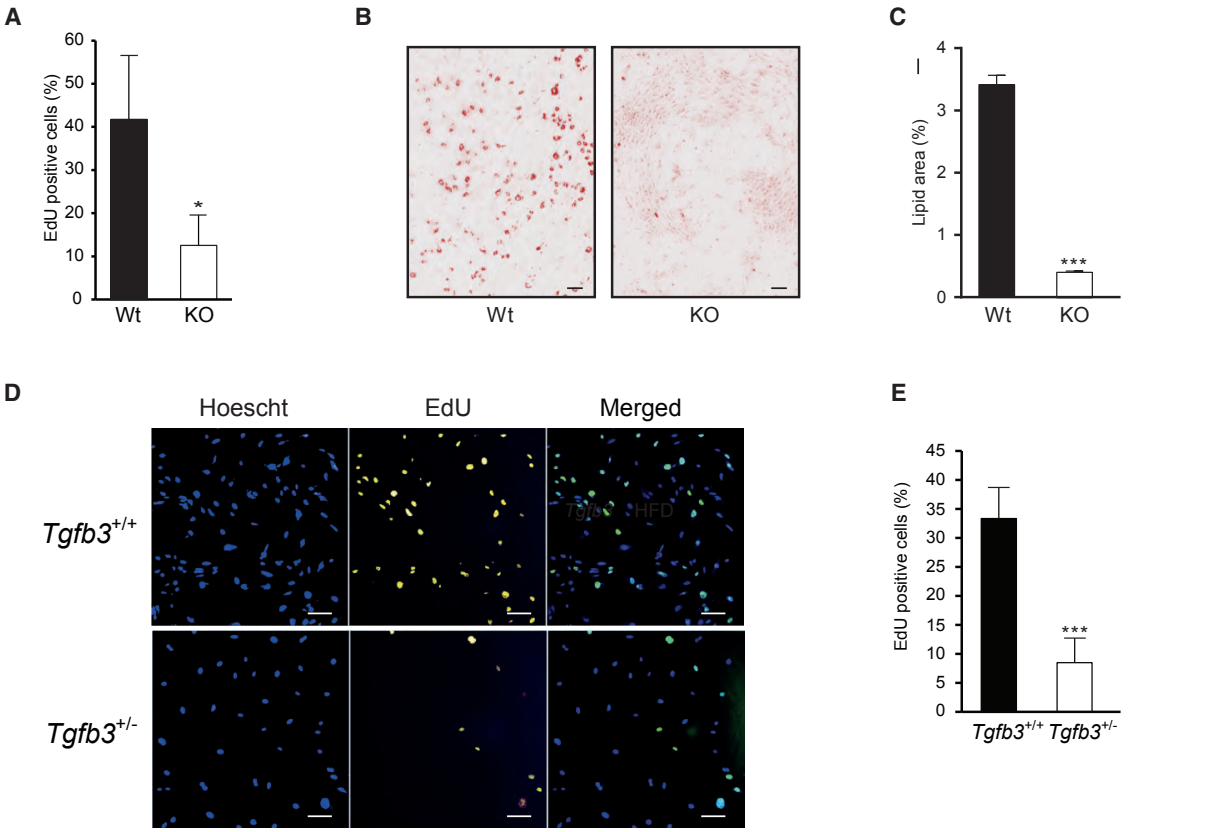

Figure 3. Effects of *Tgfb3* Depletion in Murine Cells

(A) Proliferation capacity of murine embryonic fibroblasts (MEFs) derived from *Tgfb3*$^{+/+}$ (WT) and *Tgfb3*$^{-/-}$ (KO) mice determined by EdU incorporation.

(B and C) Adipogenic differentiation of WT and KO MEFs was determined by oil red O staining (B) and triglyceride accumulation quantified using ImageJ (C).

(D) Primary cells from the stroma vascular fraction of *Tgfb3*$^{+/+}$ or *Tgfb3*$^{+/-}$ animals were cultured in the presence of EdU for 24 hr. Cells were stained for nuclei (Hoescht) and EdU (Alexa Fluor 647), and merged panels are shown at right.

(E) The fraction of EdU-positive cells was determined and quantified using ImageJ. ***$p < 0.001$, *$p < 0.05$. Scale bars, 100 μm. Error bars in (A), (C), and (E) are SD.

Expression of TGFB Members and Their Receptors in Cells of Human Subcutaneous Adipose Tissue

Expression analyses of fractionated sWAT confirmed that all three described TGFβ3 receptor genes (*TGFBR1*, *TGFBR2*, and *ACVRL1*) (Laverty et al., 2009) were present in resident WAT cells, two of which (*TGFBR2* and *ACVRL1*) were enriched in adipocyte progenitors (Figure S1G). Further analyses in the same dataset demonstrated that *TGFB2* and *-3* were most highly expressed in progenitor cells, while *TGFB1* was particularly prominent in leukocytes (Figure S1H). Data at the single-cell level (Acosta et al., 2017) confirmed an enrichment of *TGFB3* in human adipocyte precursor cells (Figure S1I).

Depleted Tgfb3 Expression Reduces Proliferation and Adipocyte Differentiation *In Vitro*

To further test the causal link between TGFβ3 and WAT morphology, studies were performed in murine *in vitro* and *in vivo* models. Mice homozygous for *Tgfb3* deletions (*Tgfb3*$^{-/-}$, knockout [KO]) die shortly after birth due to cleft palate and defects in pulmonary development (Kaartinen et al., 1995; Proetzel et al., 1995). We therefore initiated our studies by establishing *Tgfb3*$^{+/+}$ (wild-type [WT]) and *Tgfb3*$^{-/-}$ (KO) murine embryonic fibroblasts (MEFs). In comparison with WT, KO MEFs displayed significantly lower proliferation rates determined by 5-ethynyl-2′-deoxyuridine (EdU) staining (Figure 3A). This resulted in fewer proliferating adipocyte precursors, as supported by the observation that adipogenic induction resulted in fewer cells undergoing adipocyte differentiation (Figures 3B, 3C, and S2A–S2C). qPCR analyses in MEFs during differentiation confirmed that *Tgfb3* was undetectable in *Tgfb3*$^{-/-}$ cells, that there was no compensatory change in the expression of *Tgfb1* or *-2*, and that the expression of *Tgfb* receptors was not affected by genotype (Figures S2D–S2I). In contrast to the findings in hASCs and primary murine adipocytes, as well as 3T3-L1 cells, recombinant Tgfβ3 did not affect the proliferation of KO MEFs (Figure S2J; see also Discussion). The experiments in MEFs were therefore complemented by analyses in primary SVF cells from WAT of WT or heterozygous *Tgfb3*$^{+/-}$ mice. This showed that the proportion of EdU^{+} proliferating cells was significantly lower in cells from *Tgfb3*$^{+/-}$ mice (Figures 3D and 3E). In line with the data in hASCs, this phenotype could be rescued by recombinant Tgfβ3 in SVF from *Tgfb3*$^{+/-}$ animals (Figure S2K).

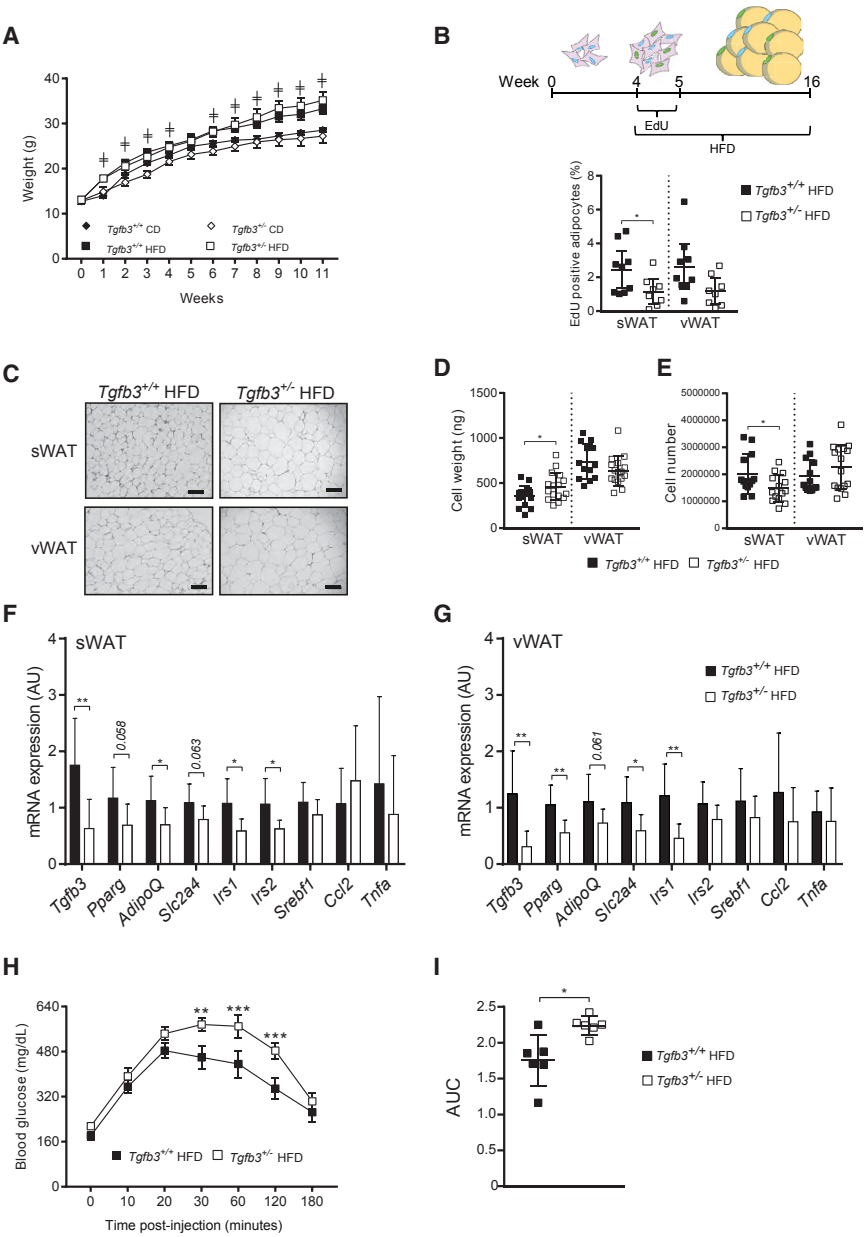

Figure 4. Diet-Induced Effects of *Tgfb3* Haploinsufficiency

(A) *Tgfb3*$^{+/+}$ and *Tgfb3*$^{+/-}$ male mice were fed chow (CD) or high-fat diet (HFD) for 11 weeks. Total body weight was determined weekly.

(B) Pulse-chase experiments were performed by administering EdU in the drinking water at weeks 4–5 (i.e., during the first week of HFD). After 11 weeks, animals were sacrificed, and inguinal (subcutaneous white adipose tissue [sWAT]) and epigonadal (vWAT) depots were obtained. Mature fat cells were isolated, and the proportion of EdU^{+} nuclei was determined by fluorescence-activated cell sorting.

(C) Representative micrographs of sWAT and vWAT from animals on HFD.

(D and E) For both depots mean adipocyte weight (D) and number (E) were assessed.

(F and G) Gene expression in sWAT (F) and vWAT (G) from animals on HFD was determined by qPCR.

(H and I) Genotype-induced effects on glucose metabolism were assessed by glucose tolerance test in animals on HFD (H). Area under the curve (AUC) was calculated (I).

In (A), ǂ denotes statistically significant difference between diets. In all of the other panels, *p < 0.05, **p < 0.01, and ***p < 0.001, using Student's t test. Scale bars, 100 μm. Error bars in (A) and (H) are SEM, and in (F)–(G), error bars are SD.

Attenuated Tgfb3 Expression Leads to sWAT Hypertrophy *In Vivo*

Given the early lethal phenotype of homozygous *Tgfb3* KO animals, *in vivo* studies were performed in *Tgfb3*$^{+/-}$ mice. These animals do not display any obvious macroscopic phenotype compared with *Tgfb3*$^{+/+}$ littermates. The impact of attenuated *Tgfb3* expression under isocaloric and hypercaloric conditions was determined by pair feeding male litters regular chow (CD) or high-fat diet (HFD) for 12 weeks (between weeks 4–16 of age), respectively. Compared to CD, HFD resulted in a more pronounced body weight increase, but there were no genotype-dependent differences in the weight attained (Figure 4A). Moreover, food intake (Figure S3A), energy expenditure (Figure S3B), respiratory exchange ratio (Figure S3C), or non-WAT organ weights (Figure S3D) were similar between genotypes. Tissue weights of sWAT and vWAT increased on HFD compared with CD, but there were no genotype differences (Figure S3D). To determine whether *Tgfb3* knockdown conferred a reduction in adipocyte precursor proliferation, we performed pulse-chase experiments with EdU during the first week of HFD (weeks 4–5 of age). Animals were then sacrificed after 11 additional weeks of HFD, and mature adipocytes were isolated from both WAT depots, followed by quantification of EdU^{+} adipocyte nuclei. This showed that *Tgfb3*$^{+/-}$ animals displayed a significantly lower proportion of EdU^{+} cells in sWAT but not in vWAT (Figure 4B). Further analyses of WAT cellularity measures were performed by determining adipocyte size and weight in histological sections of the two depots following CD (Figures S4A and S4B) and HFD (Figures 4C and 4D). In both genotypes, HFD increased adipocyte size significantly in sWAT and vWAT. The effect in vWAT was comparable between genotypes (compare Figures 4D and S4B). However, in sWAT of *Tgfb3*$^{+/-}$ animals, fat cell size was significantly larger, a difference already evident on CD (Figures S4A and S4B). Thus, *Tgfb3*$^{+/-}$ mice fed a CD had a fat cell size that was comparable to that of WT animals on HFD, with subcutaneous adipocyte size increasing even further upon HFD (Figure 4D). In concordance with other studies (see Introduction),

vWAT but not sWAT displayed an increase in fat cell number upon HFD (Figures 4E and S4C). Independent of diet, *Tgfb3*$^{+/-}$ animals displayed almost 50% fewer subcutaneous fat cells compared with WT littermates. This confirmed that the *Tgfb3*$^{+/-}$ animals were characterized by a significant, depot-specific hypertrophy in sWAT. qPCR analyses of the WAT depots in animals fed CD (Figures S4D and S4E) or HFD (Figures 4F and 4G) confirmed that haploinsufficient mice expressed ~50% lower *Tgfb3* mRNA levels in both WAT depots. Further expression analyses were performed on genes related to adipocytes (*Pparg* and *Adipoq*), insulin response (*Slc2a4*, *Irs1*, *Irs2*, and *Srebf1*), and inflammation (*Ccl2* and *Tnfa*). While there were no specific differences between genotypes on CD, several genes were significantly (*Adipoq*, *Irs1*, and *Irs2*) or borderline significantly (*Pparg* and *Slc2a4*) lower in the *Tgfb3*$^{+/-}$ animals. These genes are known to be downregulated in hypertrophic WAT (Gao et al., 2014). The effects on gene expression were specific to WAT because no genotype-related differences were observed in liver or skeletal muscle (Figures S4F and S4G) in either diet.

sWAT Hypertrophy Associates with Glucose Intolerance upon High-Fat Diet

To determine whether the differences in WAT cellularity conferred any metabolic consequences, we performed insulin tolerance (Figures S4H and S4I) and glucose tolerance tests (Figures 4H and S4J). As expected, HFD worsened insulin resistance (Figures S4H and S4I) and induced glucose intolerance (compare Figure 4H with Figure S4J). However, while there was no genotype-linked difference in the insulin tolerance tests (which primarily reflect insulin sensitivity in skeletal muscle), glucose tolerance tests showed that *Tgfb3*$^{+/-}$ mice on HFD displayed significantly larger glycemic excursions (Figures 4H and 4I). Thus, reduced *Tgfb3* expression induced sWAT hypertrophy and, upon HFD feeding, also glucose intolerance.

DISCUSSION

Several organs have the capacity to increase their size via hypertrophy and/or hyperplasia, resulting in phenotypes that are retained after pronounced tissue loss. In particular, the term "skeletal muscle memory" refers to the observation that muscle fibers that have once been hypertrophic display an improved capacity to regain mass compared to naive fibers (Gundersen, 2016). Our long-term prospective data demonstrate that human WAT expands through a combination of both increased fat cell size and number but that only the former is reversed after weight loss. Given that adipocytes are continuously turned over, this indicates a "hyperplastic" memory in WAT following tissue expansion. In an attempt to clarify mechanisms that control the observed changes, we performed transcriptomic profiling to link gene expression to fat cell number. This enabled us to identify the secreted GF TGFβ3, which accelerated human and murine fat cell formation *in vitro*. *In vivo* studies showed that *Tgfb3*$^{+/-}$ mice displayed hypertrophic sWAT, which was associated with impaired glucose metabolism upon HFD. This is in line with clinical studies that primarily link sWAT hypertrophy to impaired glucose metabolism (Hoffstedt et al., 2010).

Our clinical and murine data indicate a depot-specific role for TGFβ3. Thus, while *TGFB3* mRNA expression was higher in the sWAT of obese individuals, the corresponding levels in vWAT were lower than they were in non-obese subjects. In line with this, *Tgfb3*$^{+/-}$ mice displayed pronounced sWAT hypertrophy under both CD and HFD compared with WT littermates, a finding that was not observed in vWAT. We admit that the mechanisms underlying this depot-specificity are not clear but that they may depend on the well-established regional variations in WAT phenotype. For instance, both intrinsic differences in the developmental lineage of adipocyte progenitors (Chau et al., 2014; Macotela et al., 2012; Sanchez-Gurmaches et al., 2015, 2016) and extrinsic differences in the microenvironment of the tissue, including vascularity, cell infiltration, and secretome and metabolic capacity (Jeffery et al., 2016), could explain the differential role of TGFβ3 in determining WAT cellularity. It should be noted that in contrast to human sWAT, the current consensus is that male murine sWAT does not display any hyperplasia upon HFD. Instead, this depot expands via hypertrophic and hyperplastic mechanisms between embryonic day (E) 13.5 and puberty (postnatal days 18–34) (Berry et al., 2016; Holtrup et al., 2017). As reviewed elsewhere (Hepler and Gupta, 2017), murine studies (Jeffery et al., 2015; Jiang et al., 2014) suggest that different adipocyte precursors are important for adipogenesis during development (embryonic and early post-natal) or in response to HFD. The observation that attenuated *Tgfb3* expression resulted in sWAT hypertrophy under both CD and HFD therefore suggests that this factor may primarily affect sWAT expansion in early postnatal stages, but that its role in WAT mass increase upon hypercaloric diet may differ between (male) mice and humans. Nevertheless, our combined data in animals and humans suggest that it affects sWAT cellularity. This does not exclude that other factors may contribute to WAT cellularity via effects on adipocyte precursor proliferation and/or differentiation (Gao et al., 2014).

Our results in primary human and murine cells suggest that the mechanisms through which TGFβ3 affect sWAT cellularity involve increased proliferation of adipocyte precursors but no direct effects on adipogenesis (i.e., the differentiation process) per se. The reduced adipogenic capacity of KO MEFs but lack of proliferative response to Tgfβ3 could depend on several factors, including depletion of adipocyte progenitors, differences in culture conditions, and/or other developmental defects that alter their response. Nevertheless, MEFs may not be ideal for these types of studies. It would be important to map *Tgfb3*-expressing and -responsive cells to improve our understanding of its possible (patho)physiological role. Further insights could be achieved by using more advanced animal models. In particular, it would be of interest to understand when Tgfβ3 is most important in murine sWAT development, but also to assess the link between dysregulated expression in adipocyte progenitors and impaired glucose metabolism. However, although TGFβ3 is enriched in adipocyte progenitors (here defined as CD45^{-}/CD34^{+}/CD31^{-}), it is also expressed in resident immune cells, which could also contribute to effects on WAT cellularity. Moreover, our single-cell analyses in adipocyte progenitors did not identify a specific cell type linked to *TGFB3* expression, and at the moment we have no data indicating *Tgfb3* expression in

specific murine precursors. These considerations, together with the fact that adipocyte precursor-specific KO models have been difficult to develop (Sanchez-Gurmaches et al., 2016), prompted us to use a whole-body haploinsufficent animal model.

In human sWAT, *TGFB3* was linked to fat cell number in a manner that was qualitatively different from that of *TGFB1* and *-2*. Furthermore, no compensatory changes in the expression of these homologs or TGFβ3 receptors (Hinck and O'Connor-McCourt, 2011) were observed upon TGFβ3 reduction (in human and murine cells either *in vitro* or *in vivo*). Thus, our data indicate that TGFβ specificity is primarily achieved via differential expression of TGFβ members. The factors increasing *TGFB3* in obesity and maintaining the levels in the post-obese state remain to be defined.

The proposed role of TGFβ3 suggested herein is further supported by a study in mice in which *Tgfb3* was overexpressed under the *Tgfb1* promoter (by replacing the coding sequence of Tgfβ1 with Tgfβ3) (Hall et al., 2013). These mice displayed smaller fat cells upon HFD and improved glucose tolerance. The clinical relevance of TGFβ3 is corroborated by a recent case report describing a *de novo* mutation in the *TGFB3* gene (C409Y), which encodes a protein variant (G1226A) that does not activate its cognate receptors (Rienhoff et al., 2013). This resulted in a complex phenotype that included a pronounced loss of sWAT. It is therefore conceivable that local TGFβ3 administration could have therapeutic potential in instances in which hyperplastic WAT growth is desirable. These instances include involuntary weight loss, in which the adipogenic machinery is still functional (e.g., cancer-related cachexia, age-related cachexia), and reconstructive surgery (e.g., following mastectomy, severe burn injuries); in both of these instances, autologous fat transplantation has had poor results (Kølle et al., 2013). The feasibility of this notion is supported by the fact that TGFβ3 has undergone a clinical development program to improve superficial scar tissue formation under the name avotermin (McCollum et al., 2011). Hence, local administration of TGFβ3 has been shown to be safe and tolerable in humans. This hypothesis needs to be tested in experiments in which Tgfb3 is given to animals, possibly followed by administration of pro-adipogenic stimuli.

A previous study suggested that inhibition of TGFβ-signaling (using a non-selective anti-Tgfβ antibody) resulted in increased thermogenesis via transition of WAT into a brown adipose tissue-like phenotype (Yadav et al., 2011). We observed no difference in *Ucp1* gene expression in white or brown adipose tissue (data not shown) and no genotype effect on the size of brown adipose tissue depots. In addition, energy expenditure and respiratory exchange ratio (a measure of substrate utilization) was not different in *Tgfb3*$^{+/-}$ animals compared with WT littermates. This suggests that TGFβ3 has a specific impact on the WAT phenotype. The latter notion is also supported by the observation that there were no genotype-dependent changes in gene expression in non-adipose tissues, including liver and skeletal muscle.

Although the clinical biopsies used in the present work were obtained from the abdominal sWAT of women, and a recent study in mice suggested that depot-specific WAT expansion is influenced by gender (Jeffery et al., 2016), there is presently no evidence in humans that these mechanisms are qualitatively different between men and women. However, given that all of the animals used herein were male, we cannot exclude gender differences in WAT depot phenotypes between *Tgfb3*$^{+/-}$ and WT mice.

Here, we report the identification of a transcriptional fingerprint that is enriched for GFs and linked to sWAT cellularity. Our *in vitro* and *in vivo* analyses suggest that among these GFs, TGFβ3 is involved in hyperplastic sWAT expandability. This is mediated via effects on adipocyte precursor cell proliferation, in which weight gain induces an irreversible increase in TGFβ3 that contributes to maintained adipocyte number following weight loss. Further studies are needed to define whether this factor may be of clinical relevance in conditions in which local or general hyperplastic WAT expansion is required.

STAR★METHODS

Detailed methods are provided in the online version of this paper and include the following:

- KEY RESOURCES TABLE
- CONTACT FOR REAGENT AND CONTACT SHARING
- EXPERIMENTAL MODEL AND SUBJECT DETAILS
  - Subjects
  - Animal studies
  - Cell culture
- METHOD DETAILS
  - Clinical examination
  - Determination of human adipocyte size and number
  - Transcriptional profiling and pathway analyses
  - RNA isolation, cDNA synthesis and real-time PCR
  - Protein secretion
  - Fluorescence Activated Cell Sorting and RNA expression analysis of WAT cell populations
  - Stimulation, differentiation and proliferation of adipocytes
  - 5-ethynyl-2′-deoxyuridine incorporation *in vitro*
  - Assessment of lipid area
  - *In vivo* EdU incorporation
  - Metabolic evaluations in mice
- QUANTIFICATION AND STATISTICAL ANALYSIS
- DATA AND MATERIALS AVAILABILITY

SUPPLEMENTAL INFORMATION

Supplemental Information includes four figures and four tables and can be found with this article online at https://doi.org/10.1016/j.celrep.2018.09.069.

ACKNOWLEDGMENTS

We thank Elisabeth Dungner, Elia Escasany, Katarina Hertel, Yvonne Widlund, Kerstin Wåhlén, and Gaby Åström for excellent technical assistance. We also thank the technicians in the animal facility of Universidad Rey Juan Carlos for their help with the experiments on mice. We would also like to acknowledge the MedH Core Flow Cytometry facility at Karolinska Institutet, supported by Karolinska Institutet/Stockholm County Council (KI/SLL) for providing cell analysis, cell sorting services, and technical expertise. This work was supported by grants from the Swedish Research Council, the Novo Nordisk Foundation (including the Tripartite Immuno-metabolism Consortium grant no. NNF15CC0018486 and the Metabolites as Drivers of Inflammation in

Metabolic Diseases [MSAM] Consortium grant no. NNF15SA0018346), CIMED, the European Association on the Study of Diabetes together with Eli Lilly, the Swedish Diabetes Foundation, the Stockholm County Council, the Diabetes Wellness Fund, and the Strategic Research Program in Diabetes at Karolinska Institutet. N.M. is funded by scholarships from the Wenner-Gren Foundation and the Marie Skłodowska-Curie Actions.

AUTHOR CONTRIBUTIONS

M.R., N.M., and P.A. conceived the study. M.R., N.M., and P.P. wrote the first version of the manuscript, which was then read and approved by all of the co-authors. A.V.-P., C.M.-A., E.M., G.M.-G., M.C., P.C., and Y.L. led the experiments performed in mice. A.K., H.G., J.L., P.H., S.L., and P.P. performed, together with M.R. and N.M., additional analyses in murine and human tissues. I.D. and J.L. contributed to the design of the flow cytometry protocols. J.R.A. performed the flow cytometry analyses. Q.L. and K.L.S. performed the EdU analyses from the pulse-chase experiments. P.P. collected and analyzed, together with N.M. and M.R., all of the data. M.R. is the guarantor of the work.

DECLARATION OF INTERESTS

The authors declare no competing interests.

Received: April 17, 2017
Revised: August 31, 2018
Accepted: September 21, 2018
Published: October 16, 2018

REFERENCES

Acosta, J.R., Joost, S., Karlsson, K., Ehrlund, A., Li, X., Aouadi, M., Kasper, M., Arner, P., Rydén, M., and Laurencikiene, J. (2017). Single cell transcriptomics suggest that human adipocyte progenitor cells constitute a homogeneous cell population. Stem Cell Res. Ther. *8*, 250.

Alligier, M., Meugnier, E., Debard, C., Lambert-Porcheron, S., Chanseaume, E., Sothier, M., Loizon, E., Hssain, A.A., Brozek, J., Scoazec, J.Y., et al. (2012). Subcutaneous adipose tissue remodeling during the initial phase of weight gain induced by overfeeding in humans. J. Clin. Endocrinol. Metab. *97*, E183–E192.

Andersson, D., Wahrenberg, H., and Löfgren, P. (2009). Beta3-adrenoceptor function and long-term changes in body weight. Int. J. Obes. *33*, 662–668.

Andersson, D.P., Thorell, A., Löfgren, P., Wirén, M., Toft, E., Qvisth, V., Riserus, U., Berglund, L., Näslund, E., Bringman, S., et al. (2014). Omentectomy in addition to gastric bypass surgery and influence on insulin sensitivity: a randomized double blind controlled trial. Clin. Nutr. *33*, 991–996.

Arner, P., Arner, E., Hammarstedt, A., and Smith, U. (2011). Genetic predisposition for type 2 diabetes, but not for overweight/obesity, is associated with a restricted adipogenesis. PLoS One *6*, e18284.

Arner, P., Andersson, D.P., Thörne, A., Wirén, M., Hoffstedt, J., Näslund, E., Thorell, A., and Rydén, M. (2013). Variations in the size of the major omentum are primarily determined by fat cell number. J. Clin. Endocrinol. Metab. *98*, E897–E901.

Arner, P., Sinha, I., Thorell, A., Rydén, M., Dahlman-Wright, K., and Dahlman, I. (2015). The epigenetic signature of subcutaneous fat cells is linked to altered expression of genes implicated in lipid metabolism in obese women. Clin. Epigenetics *7*, 93.

Berry, D.C., Jiang, Y., and Graff, J.M. (2016). Emerging roles of adipose progenitor cells in tissue development, homeostasis, expansion and thermogenesis. Trends Endocrinol. Metab. *27*, 574–585.

Björntorp, P., Carlgren, G., Isaksson, B., Krotkiewski, M., Larsson, B., and Sjöström, L. (1975). Effect of an energy-reduced dietary regimen in relation to adipose tissue cellularity in obese women. Am. J. Clin. Nutr. *28*, 445–452.

Chau, Y.Y., Bandiera, R., Serrels, A., Martínez-Estrada, O.M., Qing, W., Lee, M., Slight, J., Thornburn, A., Berry, R., McHaffie, S., et al. (2014). Visceral and subcutaneous fat have different origins and evidence supports a mesothelial source. Nat. Cell Biol. *16*, 367–375.

Dahlman, I., Sinha, I., Gao, H., Brodin, D., Thorell, A., Rydén, M., Andersson, D.P., Henriksson, J., Perfilyev, A., Ling, C., et al. (2015). The fat cell epigenetic signature in post-obese women is characterized by global hypomethylation and differential DNA methylation of adipogenesis genes. Int. J. Obes. *39*, 910–919.

Gao, H., Mejhert, N., Fretz, J.A., Arner, E., Lorente-Cebrián, S., Ehrlund, A., Dahlman-Wright, K., Gong, X., Strömblad, S., Douagi, I., et al. (2014). Early B cell factor 1 regulates adipocyte morphology and lipolysis in white adipose tissue. Cell Metab. *19*, 981–992.

Garaulet, M., Hernandez-Morante, J.J., Lujan, J., Tebar, F.J., and Zamora, S. (2006). Relationship between fat cell size and number and fatty acid composition in adipose tissue from different fat depots in overweight/obese humans. Int. J. Obes. *30*, 899–905.

Goldrick, R.B., and McLoughlin, G.M. (1970). Lipolysis and lipogenesis from glucose in human fat cells of different sizes. Effects of insulin, epinephrine, and theophylline. J. Clin. Invest. *49*, 1213–1223.

Gundersen, K. (2016). Muscle memory and a new cellular model for muscle atrophy and hypertrophy. J. Exp. Biol. *219*, 235–242.

Hall, B.E., Wankhade, U.D., Konkel, J.E., Cherukuri, K., Nagineni, C.N., Flanders, K.C., Arany, P.R., Chen, W., Rane, S.G., and Kulkarni, A.B. (2013). Transforming growth factor-β3 (TGF-β3) knock-in ameliorates inflammation due to TGF-β1 deficiency while promoting glucose tolerance. J. Biol. Chem. *288*, 32074–32092.

Hepler, C., and Gupta, R.K. (2017). The expanding problem of adipose depot remodeling and postnatal adipocyte progenitor recruitment. Mol. Cell. Endocrinol. *445*, 95–108.

Hinck, A.P., and O'Connor-McCourt, M.D. (2011). Structures of TGF-β receptor complexes: implications for function and therapeutic intervention using ligand traps. Curr. Pharm. Biotechnol. *12*, 2081–2098.

Hirsch, J., and Batchelor, B. (1976). Adipose tissue cellularity in human obesity. Clin. Endocrinol. Metab. *5*, 299–311.

Hoffstedt, J., Arner, E., Wahrenberg, H., Andersson, D.P., Qvisth, V., Löfgren, P., Rydén, M., Thörne, A., Wirén, M., Palmér, M., et al. (2010). Regional impact of adipose tissue morphology on the metabolic profile in morbid obesity. Diabetologia *53*, 2496–2503.

Hoffstedt, J., Andersson, D.P., Eriksson Hogling, D., Theorell, J., Näslund, E., Thorell, A., Ehrlund, A., Rydén, M., and Arner, P. (2017). Long-term protective changes in adipose tissue after gastric bypass. Diabetes Care *40*, 77–84.

Holtrup, B., Church, C.D., Berry, R., Colman, L., Jeffery, E., Bober, J., and Rodeheffer, M.S. (2017). Puberty is an important developmental period for the establishment of adipose tissue mass and metabolic homeostasis. Adipocyte *6*, 224–233.

Jeffery, E., Church, C.D., Holtrup, B., Colman, L., and Rodeheffer, M.S. (2015). Rapid depot-specific activation of adipocyte precursor cells at the onset of obesity. Nat. Cell Biol. *17*, 376–385.

Jeffery, E., Wing, A., Holtrup, B., Sebo, Z., Kaplan, J.L., Saavedra-Peña, R., Church, C.D., Colman, L., Berry, R., and Rodeheffer, M.S. (2016). The adipose tissue microenvironment regulates depot-specific adipogenesis in obesity. Cell Metab. *24*, 142–150.

Jiang, Y., Berry, D.C., Tang, W., and Graff, J.M. (2014). Independent stem cell lineages regulate adipose organogenesis and adipose homeostasis. Cell Rep. *9*, 1007–1022.

Kaartinen, V., Voncken, J.W., Shuler, C., Warburton, D., Bu, D., Heisterkamp, N., and Groffen, J. (1995). Abnormal lung development and cleft palate in mice lacking TGF-beta 3 indicates defects of epithelial-mesenchymal interaction. Nat. Genet. *11*, 415–421.

Kølle, S.F., Fischer-Nielsen, A., Mathiasen, A.B., Elberg, J.J., Oliveri, R.S., Glovinski, P.V., Kastrup, J., Kirchhoff, M., Rasmussen, B.S., Talman, M.L., et al. (2013). Enrichment of autologous fat grafts with ex-vivo expanded adipose tissue-derived stem cells for graft survival: a randomised placebo-controlled trial. Lancet *382*, 1113–1120.

Krotkiewski, M., Björntorp, P., Sjöström, L., and Smith, U. (1983). Impact of obesity on metabolism in men and women. Importance of regional adipose tissue distribution. J. Clin. Invest. *72*, 1150–1162.

Laverty, H.G., Wakefield, L.M., Occleston, N.L., O'Kane, S., and Ferguson, M.W. (2009). TGF-beta3 and cancer: a review. Cytokine Growth Factor Rev. *20*, 305–317.

Löfgren, P., Andersson, I., Adolfsson, B., Leijonhufvud, B.M., Hertel, K., Hoffstedt, J., and Arner, P. (2005). Long-term prospective and controlled studies demonstrate adipose tissue hypercellularity and relative leptin deficiency in the postobese state. J. Clin. Endocrinol. Metab. *90*, 6207–6213.

Macotela, Y., Emanuelli, B., Mori, M.A., Gesta, S., Schulz, T.J., Tseng, Y.H., and Kahn, C.R. (2012). Intrinsic differences in adipocyte precursor cells from different white fat depots. Diabetes *61*, 1691–1699.

McCollum, P.T., Bush, J.A., James, G., Mason, T., O'Kane, S., McCollum, C., Krievins, D., Shiralkar, S., and Ferguson, M.W. (2011). Randomized phase II clinical trial of avotermin versus placebo for scar improvement. Br. J. Surg. *98*, 925–934.

Medina-Gomez, G., Gray, S.L., Yetukuri, L., Shimomura, K., Virtue, S., Campbell, M., Curtis, R.K., Jimenez-Linan, M., Blount, M., Yeo, G.S., et al. (2007). PPAR gamma 2 prevents lipotoxicity by controlling adipose tissue expandability and peripheral lipid metabolism. PLoS Genet. *3*, e64.

Proetzel, G., Pawlowski, S.A., Wiles, M.V., Yin, M., Boivin, G.P., Howles, P.N., Ding, J., Ferguson, M.W., and Doetschman, T. (1995). Transforming growth factor-beta 3 is required for secondary palate fusion. Nat. Genet. *11*, 409–414.

Rienhoff, H.Y., Jr., Yeo, C.Y., Morissette, R., Khrebtukova, I., Melnick, J., Luo, S., Leng, N., Kim, Y.J., Schroth, G., Westwick, J., et al. (2013). A mutation in TGFB3 associated with a syndrome of low muscle mass, growth retardation, distal arthrogryposis and clinical features overlapping with Marfan and Loeys-Dietz syndrome. Am. J. Med. Genet. A. *161A*, 2040–2046.

Rosen, E.D., and Spiegelman, B.M. (2014). What we talk about when we talk about fat. Cell *156*, 20–44.

Rydén, M., Agustsson, T., Laurencikiene, J., Britton, T., Sjölin, E., Isaksson, B., Permert, J., and Arner, P. (2008). Lipolysis–not inflammation, cell death, or lipogenesis–is involved in adipose tissue loss in cancer cachexia. Cancer *113*, 1695–1704.

Salans, L.B., Horton, E.S., and Sims, E.A. (1971). Experimental obesity in man: cellular character of the adipose tissue. J. Clin. Invest. *50*, 1005–1011.

Samocha-Bonet, D., Campbell, L.V., Viardot, A., Freund, J., Tam, C.S., Greenfield, J.R., and Heilbronn, L.K. (2010). A family history of type 2 diabetes increases risk factors associated with overfeeding. Diabetologia *53*, 1700–1708.

Sanchez-Gurmaches, J., Hsiao, W.Y., and Guertin, D.A. (2015). Highly selective in vivo labeling of subcutaneous white adipocyte precursors with Prx1-Cre. Stem Cell Reports *4*, 541–550.

Sanchez-Gurmaches, J., Hung, C.M., and Guertin, D.A. (2016). Emerging complexities in adipocyte origins and identity. Trends Cell Biol. *26*, 313–326.

Spalding, K.L., Arner, E., Westermark, P.O., Bernard, S., Buchholz, B.A., Bergmann, O., Blomqvist, L., Hoffstedt, J., Näslund, E., Britton, T., et al. (2008). Dynamics of fat cell turnover in humans. Nature *453*, 783–787.

Tchoukalova, Y.D., Harteneck, D.A., Karwoski, R.A., Tarara, J., and Jensen, M.D. (2003). A quick, reliable, and automated method for fat cell sizing. J. Lipid Res. *44*, 1795–1801.

Tchoukalova, Y.D., Koutsari, C., Karpyak, M.V., Votruba, S.B., Wendland, E., and Jensen, M.D. (2008). Subcutaneous adipocyte size and body fat distribution. Am. J. Clin. Nutr. *87*, 56–63.

Tchoukalova, Y.D., Votruba, S.B., Tchkonia, T., Giorgadze, N., Kirkland, J.L., and Jensen, M.D. (2010). Regional differences in cellular mechanisms of adipose tissue gain with overfeeding. Proc. Natl. Acad. Sci. USA *107*, 18226–18231.

Tudela, C., Formoso, M.A., Martínez, T., Pérez, R., Aparicio, M., Maestro, C., Del Río, A., Martínez, E., Ferguson, M., and Martínez-Alvarez, C. (2002). TGF-beta3 is required for the adhesion and intercalation of medial edge epithelial cells during palate fusion. Int. J. Dev. Biol. *46*, 333–336.

Wang, J., Duncan, D., Shi, Z., and Zhang, B. (2013a). WEB-based GEne SeT AnaLysis Toolkit (WebGestalt): update 2013. Nucleic Acids Res. *41*, W77–W83.

Wang, Q.A., Tao, C., Gupta, R.K., and Scherer, P.E. (2013b). Tracking adipogenesis during white adipose tissue development, expansion and regeneration. Nat. Med. *19*, 1338–1344.

Weyer, C., Foley, J.E., Bogardus, C., Tataranni, P.A., and Pratley, R.E. (2000). Enlarged subcutaneous abdominal adipocyte size, but not obesity itself, predicts type II diabetes independent of insulin resistance. Diabetologia *43*, 1498–1506.

Yadav, H., Quijano, C., Kamaraju, A.K., Gavrilova, O., Malek, R., Chen, W., Zerfas, P., Zhigang, D., Wright, E.C., Stuelten, C., et al. (2011). Protection from obesity and diabetes by blockade of TGF-β/Smad3 signaling. Cell Metab. *14*, 67–79.

STAR★METHODS

KEY RESOURCES TABLE

REAGENT or RESOURCE	SOURCE	IDENTIFIER
Biological Samples		
Human subcutaneous and visceral fat biopsies	This paper	N/A
Murine WAT and other tissues from wt and Tgfb3 heterozygous KO mice	This paper	N/A
Human *in vitro* differentiated adipocytes	This paper and previous work from the group	Gao et al., 2014 (PMID 28470788)
Chemicals, Peptides, and Recombinant Proteins		
3-[4,5-dimethylthiazol-2-yl]-2,5 diphenyltetrazolium bromide (MTT)	Sigma-Aldrich	M2128
Human CXCL12	Abnova Corp	P4566
Human FGF7	R&D Systems	251-KG-010
Human OGN	OriGene Technologies	TP323948
Human TGFβ3	R&D Systems	243-B3-002
Murine Tgfβ3	ProSpec	CYT-143
Critical Commercial Assays		
ELISA against human CXCL12	R&D Systems	DSA00
ELISA against human FGF7	R&D Systems	DKG00
ELISA against human OGN	Cloud-Clone Corp	SEC688Hu
ELISA against human PDGFD	USCN Life Science	E92919Hu
ELISA against human TGFβ3	Cloud-Clone	SEB949Hu
ELISA against murine Tgfβ3	MyBiosource	MBS700631
Click-iT Plus EdU Alexa Fluor 647 Flow Cytometry Assay Kit	Life technologies	C10634
Deposited Data		
Human gene expression data	This paper	GEO: GSE59034
Experimental Models: Cell Lines		
Non-immortalized MEFs from wildtype and homozygous Tgfb3 KO mice	This paper	N/A
3T3-L1 cells		N/A
Experimental Models: Organisms/Strains		
Mouse C57/BL/6J Wt and Tgfb3 Hz	Jackson Laboratories	N/A
Oligonucleotides		
TaqMan probe human*18S* rRNA	Applied Biosystems	Hs99999901_s1
TaqMan probe human *CXCL12*	Applied Biosystems	Hs00171022_m1
TaqMan probe human *FGF7*	Applied Biosystems	Hs00384281_m1
TaqMan probe human *LRP10*	Applied Biosystems	Hs00204094_m1
TaqMan probe human *OGN*	Applied Biosystems	Hs00247901_m1
TaqMan probe human *PDGFD*	Applied Biosystems	Hs00228671_m1
TaqMan probe human *TGFB3*	Applied Biosystems	Hs01086000_m1
PCR primers murine *Tgfb3* (F-GGTTACTATGCCAACTTCTG and R-CACATAGTACAAGATGGTCAG)	Sigma-Aldrich	N/A
PCR primers murine *Ckm* (F-ACAAAAGCTTCCTTGTGTG and R-AGATCTCCTCAATCTTCTGC)	Sigma-Aldrich	N/A
TaqMan probe murine *Adipoq*	Applied Biosystems	Mm00456425_m1
TaqMan probe murine *Ap2*	Applied Biosystems	Mm00445878_m1
TaqMan probe murine *Ccl2*	Applied Biosystems	Mm00441242_m1

(*Continued on next page*)

Continued

REAGENT or RESOURCE	SOURCE	IDENTIFIER
TaqMan probe murine *Cidec*	Applied Biosystems	Mm00617672_m1
TaqMan probe murine *Irs1*	Applied Biosystems	Mm01278327_m1
TaqMan probe murine *Irs2*	Applied Biosystems	Mm03038438_m1
TaqMan probe murine *Plin*	Applied Biosystems	Mm00558672_m1
TaqMan probe murine *Pparg*	Applied Biosystems	Mm00440940_m1
TaqMan probe murine *Slc2a2*	Applied Biosystems	Mm00446229_m1
TaqMan probe murine *Slc2a4*	Applied Biosystems	Mm00436615_m1
TaqMan probe murine *Srebf1*	Applied Biosystems	Mm00550338_m1
TaqMan probe murine *Tnfa*	Applied Biosystems	Mm00443258_m1
TaqMan probe murine *18S* rRNA	Applied Biosystems	Mm03928990_g1
siRNA anti human TGFB3 (ON-TARGETplus)	Dharmacon	L-019740-00-0005
siRNA Non-silencing control (ON-TARGETplus)	Dharmacon	D-001810-10-05
Software and Algorithms		
ImageJ 1.45 software	NIH	N/A
GraphPad Prism 7.0	GraphPad Software	N/A
SPSS v24	IBM	N/A

CONTACT FOR REAGENT AND CONTACT SHARING

Further information and requests for resources and reagents should be directed to and will be fulfilled by the Lead Contact, Mikael Rydén, mikael.ryden@ki.se.

EXPERIMENTAL MODEL AND SUBJECT DETAILS

Subjects

Three cohorts were investigated. Cohort 1 comprised 85 healthy non-obese women recruited 1987-2000 in a study of subcutaneous adipocytes (Andersson et al., 2009). They were contacted by letter and asked for a re-investigation starting from 1997, which was before established rules for trial registrations. Thirty-eight women agreed and those who reported either stable or increased body weight (n = 27) underwent a second adipocyte examination during the period 1998-2007. Cohort 2 consisted of 81 obese women scheduled for gastric by-pass surgery (Roux-en-Y) between 2006-2009 (Clinical Trial Registration number: NCT01785134) (Andersson et al., 2014). They were post-operatively re-examined at our research unit after two years; 21 had reduced their body mass index (BMI) to a non-obese level (< 30 kg/m^2), herein defined as a post-obese state. Subjects were asked for their body weight development during childhood and adolescence as well as their BMI at 18 years of age. Among the 21 post-obese individuals, eleven reported early- (< 18 years) and ten late- (> 18 years) onset of excess weight gain (BMI > 25 kg/m^2). For each post-obese subject, we recruited a female matched for age and current BMI who had never been obese (Cohort 3). At each time of investigation all subjects were weight stable (±2 kg) for at least 3 months according to self-report. The study was approved by the regional board on ethics. It was explained in detail to each participant and written informed consent was obtained.

Animal studies

The generation of the original *Tgfb3* KO model has been described previously (Proetzel et al., 1995). Age-matched male C57/BL/6J Wt (*Tgfb3*$^{+/+}$) and Hz (*Tgfb3*$^{+/-}$) mice (Tudela et al., 2002) (Jackson Laboratories, Bar Harbour, ME) were housed in climate-controlled quarters with a 12-hour light/dark cycle. Food and water were available *ad libitum*. Mice were fed either a standard chow diet (13% of calories derived from fat 2014C, Research Diets; Harlan Laboratories) or a 29% fat diet (Teklad Custom Diet). Animals were handled following the European Union laws and guidelines for animal care. Experimental procedures were approved by the Universidad Rey Juan Carlos ethical committee (Madrid, Spain), and special care was taken to minimize animal suffering and to reduce the number of animals used. Animals were sacrificed by cervical dislocation, total body weight assessed and WAT obtained from subcutaneous periinguinal (sWAT), perirenal (pWAT) and epididymal/perigonadal (vWAT) regions. Other tissues (brown adipose tissue, pancreas, kidney, skeletal muscle and liver) were also dissected. The wet weight of each dissected tissue was measured. Thereafter, one part was fixed in 4% formalin (pH = 7.0) and used for histological analyses while the remaining specimens were frozen (−80°C) immediately after removal for subsequent RNA isolation. Determination of adipocyte size was performed exactly as detailed previously (Gao et al., 2014). In brief, fixed tissues were embedded in paraffin before being sectioned (5 μm) and stained with hematoxylin and eosin (H & E; Sigma-Aldrich). For each sample, representative photomicrographs were acquired blindly with regard to

genotype/diet from the whole section using the CellInsight CX5 High Content Screening (HCS) Platform (4X magnification). Average adipocyte size (Feret's diameter) in each animal was assessed using the ImageJ 1.45 software (National Institutes of Health, Bethesda, MD, USA) and the macro MRI's adipocyte tool. The procedure was performed by two independent operators with similar results obtained (data not shown). Adipocyte number was calculated by dividing the WAT tissue weight with mean fat cell weight as described above.

Cell culture

Cultures of hASCs as well as primary cells from the stromal-vascular fraction (SVF) were setup, cultured and differentiated as described (Gao et al., 2014). In brief, hASCs were obtained from abdominal sWAT of one male donor. Human SVF was obtained from sWAT of otherwise healthy subjects undergoing cosmetic surgery. In these subjects only BMI, age and gender was known. All subjects gave informed written consent to donate the tissue and the study is approved by the regional board on ethics. Primary mouse SVF, 3T3-L1 cells and Murine Embryonic Fibroblasts (MEFs) were handled according to the instructions from American Type Culture Collection (Manassas, VA). MEFs were cultured in high glucose DMEM containing 10% FBS, 2 mM glutamine, 0.1 mM 2-mercaptoethanol, 50 U/mM penicillin and 50 mg/mL streptomycin. Adipogenesis was induced two days post confluence using DMEM/F12 Glutamax I containing 10% fetal bovine serum (FBS) supplemented with 5 μg/mL insulin, 0.25 μmol/L dexamethasone, 0.5mmol/L 3-isobutyl-1-methylxanthine (IBMX) and 10 μmol/L rosiglitazone for two days after which the dexamethasone and IBMX were removed and the cells were allowed to undergo full adipogenic differentiation.

METHOD DETAILS

Clinical examination

After an overnight fast, anthropometric measures (height, weight, waist and hip circumferences) were determined and venous blood samples were obtained for routine clinical chemistry analyses. Body composition was determined by bioimpendance (Tanita Co, Tokyo, Japan) for Cohort 1 and by dual-X-ray absorptiometry (GE Luna iDXA, GE Health Care, Madison, WI) for Cohort 2 and 3 as described (Arner et al., 2013). Finally, a sWAT biopsy was obtained from the para-umbilical region by needle aspiration under local anesthesia.

Determination of human adipocyte size and number

Methods for determination of WAT cellularity have been described in detail previously (Arner et al., 2013). In brief, isolated adipocytes were prepared by collagenase incubation. The diameter of 100 cells were determined and shown to be normally distributed. Using established formulae (Goldrick and McLoughlin, 1970), these values were used to calculate average size and weight of the adipocytes in the WAT biopsy. The precision of the measures is not improved by increasing the number of counted cells (Tchoukalova et al., 2003) and is comparable to estimating cell size in intact tissue by histology, as discussed previously (Arner et al., 2013). The total number of adipocytes in the body was determined by dividing body fat mass by mean adipocyte weight. A limitation of this method is that there are some differences in mean adipocyte volume and weight between fat depots as well as within the subcutaneous depot (Björntorp et al., 1975; Garaulet et al., 2006; Krotkiewski et al., 1983; Tchoukalova et al., 2008). Nevertheless, the regional differences are negligible and there is a strong relationship in adipocyte size between different depots in the same individual (Garaulet et al., 2006; Krotkiewski et al., 1983; Tchoukalova et al., 2008).

Transcriptional profiling and pathway analyses

In a subgroup of cohort 2 (before and after surgery, n = 16) and 3 (matched never-obese controls, n = 16), total RNA was isolated from intact sWAT and gene expression profiles generated using Affymetrix Human Gene 1.1 arrays (Affymetrix, Inc., Santa Clara, CA) as described (Arner et al., 2015; Dahlman et al., 2015). Results were thereafter preprocessed with the Robust Multichip Average method. Principal component analysis was performed using the FactomineR package. To identify differentially regulated genes comparing subgroups, significance analysis of microarrays (SAM), with a false discovery rate (FDR) of 1%, was performed. Sets of genes (maximally the 200 most strongly regulated) displaying similar expression patterns were subjected to pathway analyses using the Web-based Gene set analysis toolkit (WebGestalt) (Wang et al., 2013a). The top ten pathways were extracted from Gene ontology, Kyoto Encyclopedia of Genes and Genomes and WikiGenes with adjusted p values < 0.01 containing more than three genes of interest were considered relevant. For retrospective analysis of previously published microarray data based on human sWAT obtained from subjects fed a lipid-enriched diet (Alligier et al., 2012), the 79 candidate genes identified in the current study were extrapolated and analyzed for differential expression using SAM. RNA was extracted from human adipocyte progenitors treated with 10 ng/mL TGFβ3 for 24 hours and analyzed by the CLARIOM-S gene microarray (Affymetrix, Inc.). Data are based on two independent experiments, each of which was run in triplicates.

RNA isolation, cDNA synthesis and real-time PCR

Total RNA was extracted from intact human or murine WAT, mature adipocytes, SVF as well as cell cultures as described previously (Gao et al., 2014). The concentration, purity and quality were measured using Nanodrop 2000 (Thermo Fisher Scientific, Lafayette, CO) and Agilent 2100 Bioanalyzer (Agilent Technologies, Palo Alto, CA). Total RNA was reverse transcribed with Omniscript RT

(QIAGEN, Hilden, Germany) with random hexamer primers (Invitrogen, Carlsbad, CA) or iScript cDNA synthesis kits (Bio-Rad, Hercules, CA). Assessments of mRNA levels were performed using TaqMan assays (Applied Biosystems, Foster City, CA) and relative expression was calculated with the comparative Ct-method, i.e., $2^{\Delta Ct\text{-target gene}}/2^{\Delta Ct\text{-reference gene}}$. The following probes were used (detailed in the Key Resources Table): *18S*, *CXCL12*, *FGF7*, *LRP10*, *OGN*, *PDGFD* and *TGFB3*. Murine gene expression was assessed using primers/probes targeting *Tgfb3*, *Ckm*, *Adipoq*, *Ap2*, *Ccl2*, *Cidec*, *Irs1*), *Irs2*, *Plin*, *Pparg*, *Slc2a2*, *Slc2a4*, *Srebf1*, *Tnfa*, and normalized against *18S rRNA*.

Protein secretion

Conditioned media was collected at day 1, 2, 3, 6, 8, 10 and 13 of human adipocyte differentiation and secreted levels of CXCL12 (DSA00, R&D Systems, Minneapolis, MN), FGF7 (DKG00, R&D Systems), OGN (SEC688Hu, Cloud-Clone Corp., Houston, TX), PDGFD (E92919Hu, USCN Life Science, Wuhan, Peoples Republic of China) and TGFβ3 (SEB949Hu, Cloud-Clone Corp.) were assessed using Enzyme-Linked Immunosorbent Assay (ELISA). Tgfβ3 secretion from murine cells was assessed by ELISA according to the manufacturer's instructions (MyBiosource, MBS700631). Samples with weaker signals than the lowest point of the standard curve were set to zero and all measurements were normalized to secretion per 24 hours.

Fluorescence Activated Cell Sorting and RNA expression analysis of WAT cell populations

The SVF and mature adipocytes were prepared from human sWAT obtained by liposuctions or plastic surgery as described (Gao et al., 2014). Fluorescence activated cell sorting (FACS) of SVF was performed as described (Acosta et al., 2017). Progenitor cells were sorted as CD45-/CD31-/CD34+, total macrophages as CD45+/CD14+/CD206+, M1 macrophages CD45+/CD14+/CD206+/CD11c+, M2 macrophages CD45+/CD14+/CD206+/CD11c-, total T cells CD45+/CD3+, CD8 T cells CD45+/CD3+/CD8+ and CD4 T cells CD45+/CD3+/CD4+. RNA Quality from total SVF, mature adipocytes, progenitor cells, leukocytes and macrophages was assessed by Agilent Bioanalyzer 2100 (Agilent Technologies Inc., Santa Clara, CA), accepting RIN > 6.6. RNA was analyzed on Clariom D Human assay (Thermo Fisher Scientific, Lafayette, CO) in accordance with the manufacturer's instructions as described (Acosta et al., 2017). The single cell mRNA analysis in human macrophages and adipocyte progenitors is described in detail in (Acosta et al., 2017).

Stimulation, differentiation and proliferation of adipocytes

hASC proliferation was estimated after addition of 1, 10 or 50/100 ng/mL recombinant human CXCL12 (P4566, Abnova Corp., Taipei City, Taiwan), FGF7 (251-KG-010, R&D Systems), OGN (TP323948, OriGene Technologies Inc., Rockville, MD), and TGFβ3 (243-B3-002, R&D Systems), by staining with 3-[4,5-dimethylthiazol-2-yl]-2,5 diphenyltetrazolium bromide (MTT, M2128, [Sigma-Aldrich, St. Louis, MO]). Briefly, ~4800 cells/cm^2 were plated in DMEM (Thermo Fisher Scientific) supplemented with 10% FBS (Thermo Fisher Scientific) and allowed to adhere for ~24 hours. Thereafter, they were washed twice with phosphate buffered saline (PBS) and cultured in DMEM with or without the recombinant proteins detailed above. Approximately 72 hours later, cells were washed twice with PBS and incubated for 60 minutes at 37 °C in DMEM containing 0.3 mg/mL MTT. Supernatants were discarded and MTT crystals were dissolved in 250 μL isopropanol. Finally, 100 μL of the lysate was transferred to 96-well plates and absorbance was measured at 592 nm. For TGFβ3, results were repeated in 3T3-L1 and murine primary adipose SVF cells using mouse recombinant protein (CYT-143, ProSpec, East Brunswick, NJ). For all experiments performed, cells cultured in DMEM supplemented with 10% FBS was used as a positive control (results not shown) and all of the steps detailed above were carried out using phenol red-free DMEM. For the *TGFB3* RNAi and rescue experiments in human adipocyte precursors, proliferating cells were transfected with non-silencing or TGFB3-specific siRNA oligonucleotides (Dharmacon, see Key Resources Table for details) using HiPerfect (QIAGEN) according to the manufacturer's instructions at day 0 and 1 after plating. Forty-eight hours after the first transfection, cells were incubated with or without increasing concentrations of recombinant human TGFβ3. Following an additional 48 hours, cell density was determined by MTT as described above. Knockdown efficiency was determined by qPCR in parallel samples (i.e 96 hours after the first transfection). The effect of recombinant murine Tgfb3 in *Tgfβ3*$^{-/-}$ (KO) MEFs was determined after 48 hours of incubation by MTT. For assessments of effects on adipogenesis in human cells, adipocyte precursor cells were incubated with or without TGFβ3 for 48 hours. Following incubation, TGFβ3 was removed and cells were incubated for 72 hours with basal medium in order for the cells to undergo clonal expansion. This was followed by induction of differentiation as described above. After differentiation, cells were fixed and stained with Oil red O and quantified as stated above.

5-ethynyl-2′-deoxyuridine incorporation *in vitro*

MEFs collected from *Tgfβ3*$^{+/+}$ (Wt) and KO mice were plated in Corning® CellBIND® T75 flasks (1 million cells/flask). One day after plating, the cells were incubated with the MEF culture media (described above) containing 10 μM 5-ethynyl-2′-deoxyuridine (EdU) for 24 hours, followed by an assessment of EdU positive cells using the Click-iT® Plus EdU Alexa Fluor® 647 Flow Cytometry Assay Kit (Life technologies, Carlsbad, CA) according to the manufacturer's instructions. Analysis was performed on a LSRFortessa equipped with 405 nm, 488 nm, 561 nm and 640 nm lasers and the Diva software (BD Biosciences).

For analyses in primary SVF from Wt and Hz mice, cells were plated in Corning® CellBIND® 96 well plates followed by incubation with 10 μM EdU for 24 hours. Cells were then fixed in the plates using 4% paraformaldehyde for 15 minutes and stained using the

Click-iT® Plus protocol. Incorporation of EdU and nuclear staining (Hoescht) were analyzed using a CellInsightCX5 High Content Screening Platform at 10X magnification and expressed as % EdU positive cells. Effects on proliferation in SVF from Hz animals were determined by the same EdU protocol after 24 hours of incubation with or without different concentrations of murine Tgfb3.

Assessment of lipid area

In vitro differentiated human adipocytes and MEFs were stained by Oil red O. Each treatment was done in triplicate. One picture per well from a random spot were acquired at 4X magnification. The Oil red O positive area in each microphotograph was quantified using ImageJ.

In vivo EdU incorporation

The mice were put on a high fat diet and given 5-ethynyl-2′-deoxyuridine (EdU) in the drinking water at a concentration of 1 mg/mL (in 2% sucrose solution to offset taste aversion) from 4 weeks of age. EdU was removed from the drinking water after 1 week and the mice continued on a high fat diet until 16 weeks of age at which point they were sacrificed. Mature adipocytes were isolated from the sWAT and eWAT as described above followed by nuclear isolation and FACS sorting. In brief, packed adipocytes were lyzed and homogenized in lysis buffer (10 mM Tris, 5nM MgCl2, 0.3M sucrose, 0.6% NP-40, and protease inhibitor cocktail (Roche)) by passing through a syringe with a 20G needle 3 times. After spinning at 16,000*g* for 1 min, crude nuclei pellets were fixed, permeabilized and stained with a Click-it EdU Alexa Fluor 488 assay according to the manufacturer's instructions (Life technologies, C10337). Samples were then rinsed in 1% BSA, resuspended in PBS containing 10 μg/mL 4,6-diamidino-2-phenylindole (DAPI, Thermo Fisher Scientific), and analyzed on a BD CytoFlex analyzer. Data analyses were performed using Flowlogic software (Miltenyi Biotec) and expressed as the percentage of DAPI positive events that were also EdU-Alexa 488 positive.

Metabolic evaluations in mice

Male animals were placed at 20°C in a comprehensive laboratory animal monitoring system attached to a custom-built oxygen and carbon dioxide monitoring system (PhenoMaster, TSE Systems, Germany). Airflow rates were 400 mL/min measurements of oxygen concentration, with carbon dioxide concentration in room air and air leaving each cage were measured every 15 min. Energy expenditure (EE) was calculated from the amount of O_2 consumed (called VO_2) and the amount of CO_2 produced (VCO_2) using the equation: EE (J) = $15.818VO_2 + 5.176VCO_2$. The respiratory exchange rate (RER) was calculated with the ratio VCO_2/VO_2. The consumed oxygen (VO_2), activity, food and drink intake of each animal were calculated with these metabolic cages. Glucose tolerance tests (GTTs) were performed as described (Medina-Gomez et al., 2007). In brief, after 16 hours of fasting glucose was administered intraperitoneally (1 g glucose/kg body weight). Blood glucose levels were monitored using a glucose meter (Boehringer) on 2.5 μL of blood obtained from the tail vein; areas under curve (AUCs) were calculated and were expressed as mean ± SEM.

QUANTIFICATION AND STATISTICAL ANALYSIS

Values are mean ± SEM. Results were evaluated using paired/unpaired t test or analysis of variance (ANOVA). Fisher's least significant difference post hoc tests were used. A statistical power calculation was made on available values for subcutaneous fat cell volume in 670 subjects investigated previously (Spalding et al., 2008). In two equally sized obese groups of subjects (10+10), we could detect a 15% difference with alpha = 0.05 and 80% power by two-sided t test. Similarly, in two equally sized non-obese groups of subjects (21+21), we had 90% power to detect a 15% difference with alpha = 0.05.

DATA AND MATERIALS AVAILABILITY

Human gene expression data are deposited in the National Center for Biotechnology Information Gene Expression Omnibus (https://www.ncbi.nlm.nih.gov/geo/), accession number GSE59034.

Cell Reports, Volume *25*

Supplemental Information

Transforming Growth Factor-β3 Regulates Adipocyte Number in Subcutaneous White Adipose Tissue

Paul Petrus, Niklas Mejhert, Patricia Corrales, Simon Lecoutre, Qian Li, Estela Maldonado, Agne Kulyté, Yamila Lopez, Mark Campbell, Juan R. Acosta, Jurga Laurencikiene, Iyadh Douagi, Hui Gao, Concepción Martínez-Álvarez, Per Hedén, Kirsty L. Spalding, Antonio Vidal-Puig, Gema Medina-Gomez, Peter Arner, and Mikael Rydén

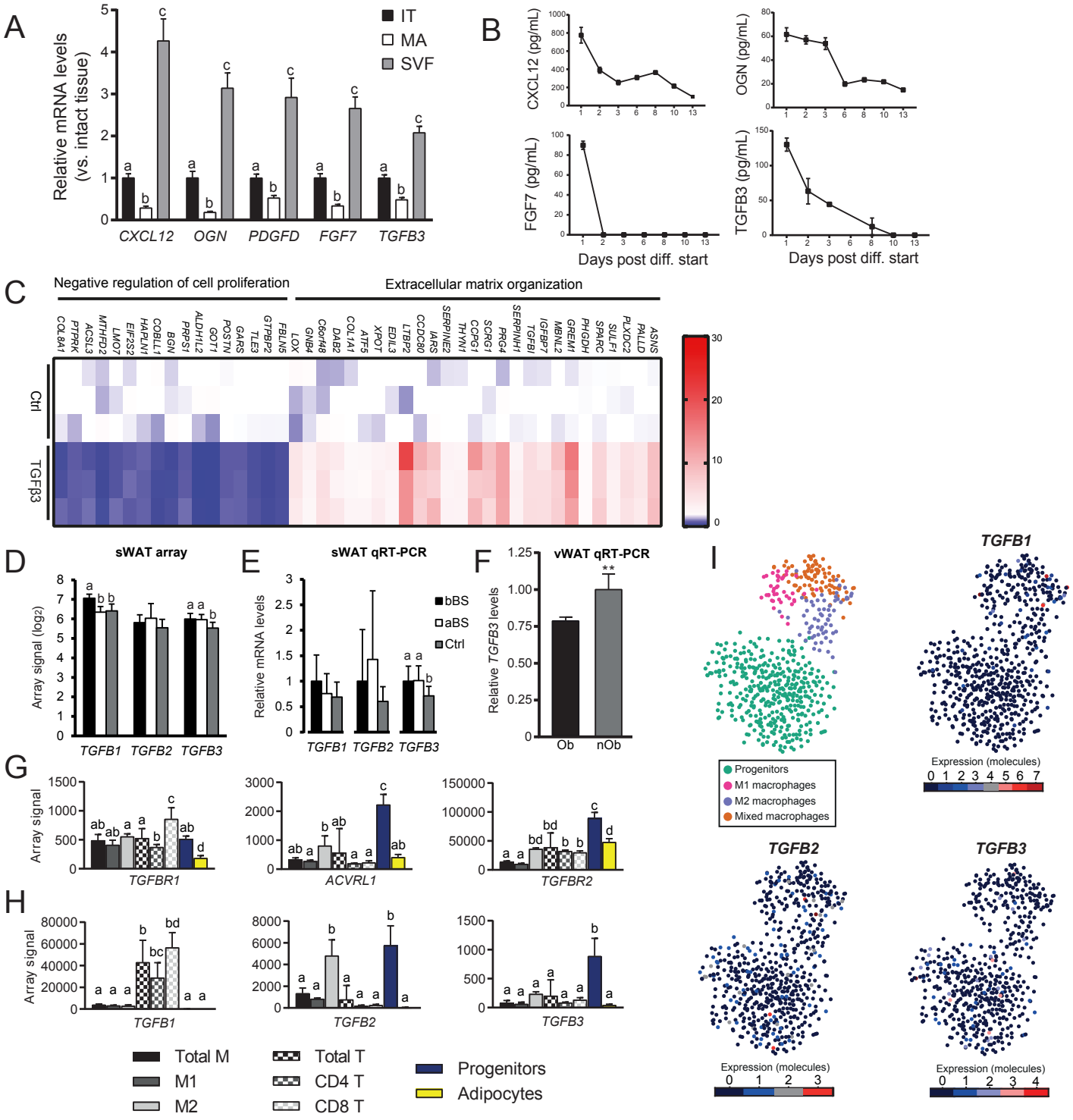

Figure S1 (related to Figure 1) *Expression of identified growth factors, TGFßs and their receptors.* **A.** Messenger RNA expression of the indicated genes in intact abdominal subcutaneous white adipose tissue (IT, black), isolated adipocytes (MA, white) and the stromal-vascular fraction (SVF, grey). **B**. Secretion of indicated growth factors from human adipocyte precursor cells during *in vitro* adipogenesis. **C.** Human adipose-derived stem cells (hASCs) were incubated with 10 ng/mL TGFβ3 or control (Ctrl) medium for 24 hours. Cells were lysed and RNA analyzed by gene microarray as shown in Figure 2. Heatmap representation of genes included in two of the top pathways, expression of individual genes in control (Ctrl) or TGFβ3-treated cells are shown. **D-E.** Messenger RNA expression of *TGFB1-3* in cohort 2 and 3 determined by micro-array (panel D) and by RT-qPCR (panel E). **F.** *TGFB3* mRNA expression determined by RT-qPCR in visceral WAT from obese (Ob) and non-obese (nOb) subjects. **G-H.** Gene expression of TGFβ receptors (G) and TGFβ ligands (H) determined by gene microarray in various cell fractions of human sWAT including: mature adipocytes and the following cells in the SVF: macrophages (M1, M2 and total), T-cells ($CD4^+$, $CD8^+$ and total) and adipocyte progenitors. The bars represent the mean array signal and error bars are standard error of the mean. **I.** T-distributed stochastic neighbor embedding (tSNE) plots of single cell gene expression in SVF cells isolated from human subcutaneous WAT. The cell populations identified are represented by the tSNE plot in the upper left panel. The macrophages can be subdivided into M1 (pink), M2 (blue) and mixed cells (orange) while adipocyte progenitors (green) cluster into a single population. The other panels show the expression of *TGFB1-3* in the populations. *TGFB3* expression is on average higher in progenitors than in macrophages and there is no distinct subpopulation within the progenitor fraction that is *TGFB3*-specific. The tSNE plots are based on previously published data (Acosta et al., 2017). In panel A, D-E and G-H, ANOVA was used to evaluate the results and statistically significant differences ($p<0.05$) between fractions are indicated by connecting letters. In panel F **=$p<0.01$, using Student's t-test. All error bars are S.D.

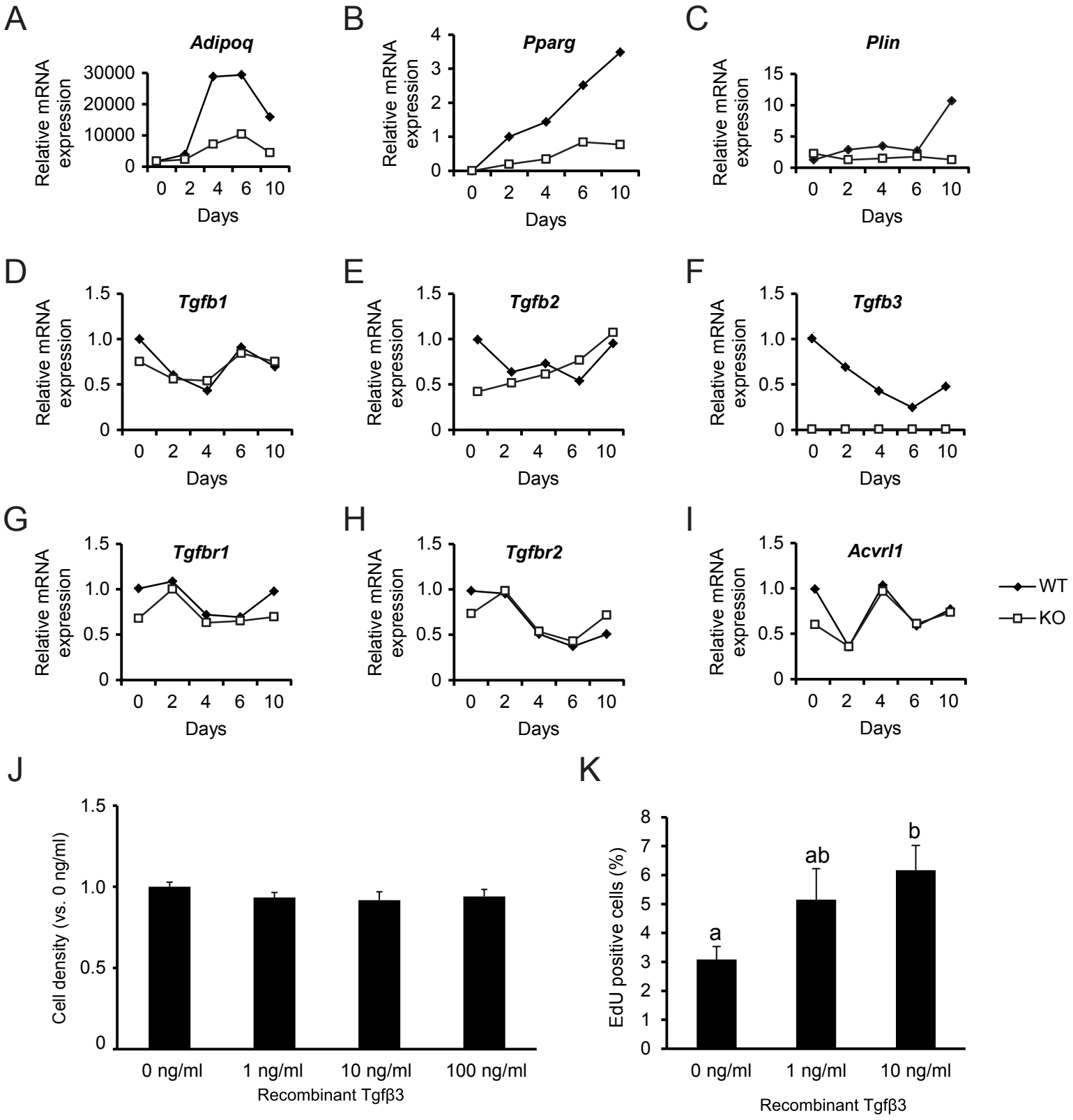

Figure S2 (related to Figure 3). *Gene expression in murine embryonic fibroblasts.* **A-I.** Adipogenesis was induced in wildtype *Tgfb3*$^{+/+}$ (WT) or *Tgfb3*$^{-/-}$ (KO) murine embryonic fibroblasts (MEFs) and the mRNA expression of adipogenic genes (**A-C**), Tgfβ1-3 (**D-F**) and Tgfβ3 receptors (**G-I**) were measured. The data points are mean expression from two independent experiments. **J.** Tgfβ3 KO MEFs were incubated with the indicated concentrations of recombinant murine Tgfβ3 and cell density was assessed by MTT staining (described in STAR Methods). **K.** Primary adipose SVF cells from *Tgfb3*$^{+/-}$ mice were incubated with the indicated concentrations of recombinant murine Tgfβ3. Proliferation was determined by EdU incorporation and expressed as % EdU positive cells as detailed in STAR Methods. Statistically significant differences ($p<0.05$) between conditions are indicated by connecting letters. All error bars are S.D.

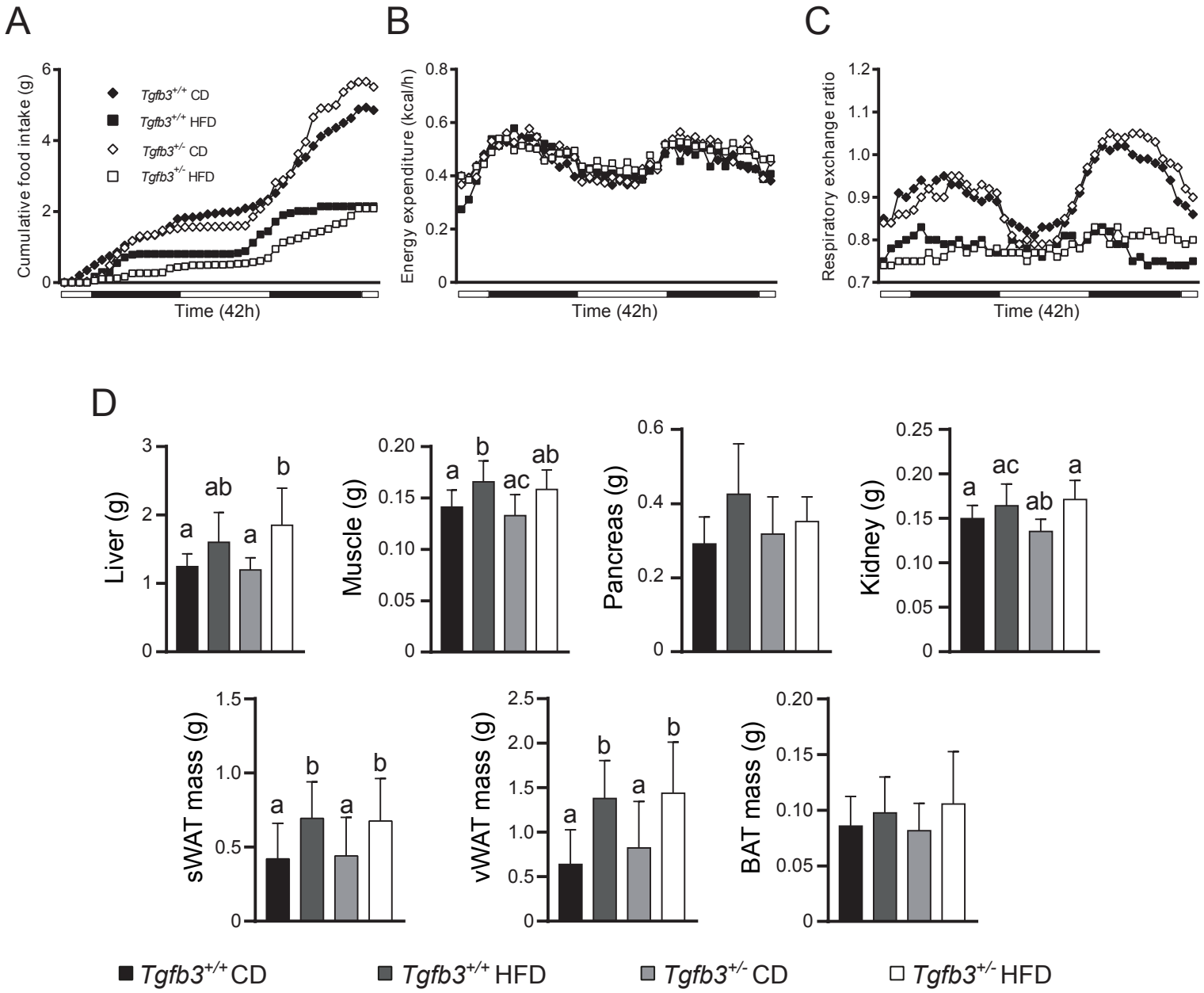

Figure S3 (related to Figure 4). *Characterization of Tgfb3$^{+/-}$ mice.* **A-C.** Wild type and Tgfb3 haploinsufficient male mice were fed chow (CD) or high-fat diet (HFD) for 11 weeks. Food intake (A), energy expenditure (B) and respiratory exchange ratio (C) was measured during a 42 h period in *Tgfb3*$^{+/+}$ and *Tgfb3*$^{+/-}$ animals on CD or HFD during the final week before euthanizing the animals. **D.** The wet-weights of liver, skeletal muscle, pancreas, kidney, perininguinal (subcutaneous) white adipose tissue (sWAT), epigonadal (visceral) white adipose tissue (vWAT) and brown adipose tissue (BAT) were compared between the groups. In panel D ANOVA was used to evaluate the results and statistically significant differences ($p<0.05$) between groups are indicated by connecting letters. All error bars are S.D.

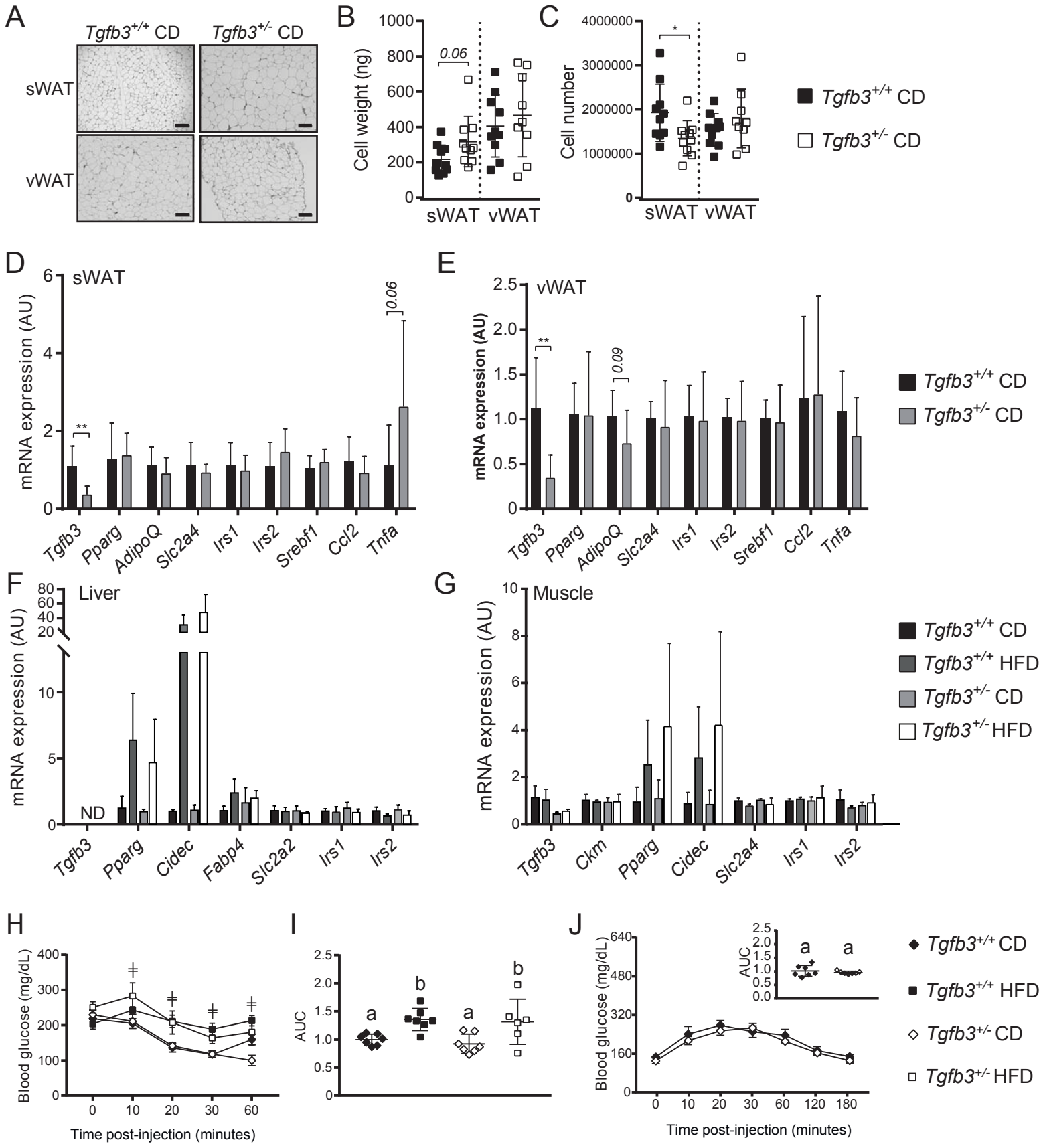

Figure S4 (related to Figure 4). *Further characterization of Tgfb3$^{+/-}$ mice.* Wild type and Tgfb3 haploinsufficient male mice were fed chow or high-fat diet (HFD) for 11 weeks. **A.** Representative microphotographs of sWAT and vWAT from animals on CD. Scale bars are 100 µm. **B-C.** For both depots mean adipocyte weight (panel B) and number (panel C) were assessed in the indicated WAT depots. **D-E.** Gene expression in sWAT (panel D) and vWAT (panel E) was determined in animals on CD. **F-G.** Gene expression in liver (panel F) and skeletal muscle (panel G) was determined by RT-qPCR in animals on CD or HFD as indicated. **H-I.** Insulin sensitivity were assessed by insulin tolerance test (ITT) in *Tgfb3*$^{+/+}$ and *Tgfb3*$^{+/-}$ mice animals on CD or HFD (panel H). Area under the curve (AUC) was calculated (panel I). In panel H, ǂ denotes statistically significant difference between diets. **J.** Glucose tolerance tests were performed in *Tgfb3*$^{+/+}$ and *Tgfb3*$^{+/-}$ mice fed CD. The AUCs are inserted. In panel C, D and E ***=p<0.001, **=p<0.01, *=p<0.05.,using Student's t-test. In panel I and J, significant differences (p<0.05) are denoted by connecting letters. Error bars in panel D-G are S.D. Error bars in panel H and J are S.E.M.

Table S1 (related to Figure 1). Clinical characteristics of Cohort 1.

	Tertile 1 - weight stable (n=9)			Tertile 2 - intermediate group (n=9)			Tertile 3 - weight gainers (n=9)		
Parameter	Baseline	Follow-up	p-value	Baseline	Follow-up	p-value	Baseline	Follow-up	p-value
Age (yr)	40.8 ± 2.8	49.9 ± 3.7	0.000	39.3 ± 3.2	50.4 ± 3.3	0.000	36.8 ± 3.6	47.1 ± 3.6	0.000
BMI (kg/m^2)	22.9 ± 0.6	22.9 ± 0.6	0.951	23.5 ± 0.6	24.6 ± 0.6	0.000	24.3 ± 1.6	28.8 ± 2.1	0.000
Waist (cm)	81.1 ± 2.7	82.0 ± 2.8	0.574	80.6 ± 2.4	89.2 ± 2.3	0.001	83.7 ± 4.2	96.5 ± 4.4	0.001
Hip (cm)	94.0 ± 2.2	95.6 ± 1.1	0.434	94.5 ± 2.7	98.2 ± 1.7	0.019	97.2 ± 3.3	106.4 ± 3.4	0.008
Waist-to-hip ratio	0.863 ± 0.024	0.857 ± 0.025	0.812	0.854 ± 0.018	0.907 ± 0.015	0.026	0.859 ± 0.021	0.904 ± 0.017	0.085
Body fat (%)	30.7 ± 1.1	30.9 ± 1.5	0.798	32.0 ± 1.9	34.4 ± 1.7	0.000	31.7 ± 3.3	40.6 ± 4.2	0.000
P-glucose (mmol/l)	4.9 ± 0.1	4.9 ± 0.1	0.820	4.9 ± 0.1	5.0 ± 0.1	0.575	5.0 ± 0.1	4.9 ± 0.1	0.782
P-insulin (mU/l)	6.1 ± 0.6	4.9 ± 0.8	0.287	5.5 ± 0.8	4.4 ± 0.7	0.111	7.6 ± 1.4	7.2 ± 1.4	1.000
Log_{10} $HOMA_{IR}$	0.1 ± 0.1	-0.0 ± 0.1	0.210	0.0 ± 0.1	-0.1 ± 0.1	0.167	0.2 ± 0.1	0.1 ± 0.1	0.981
P-triglycerides (mmol/l)	0.8 ± 0.1	0.9 ± 0.1	0.194	0.9 ± 0.3	0.9 ± 0.2	0.963	1.0 ± 0.1	1.2 ± 0.3	0.238

Abbreviations: BMI, body mass index; $HOMA_{IR}$, homeostatic model assessment

Values are mean ± SEM

Table S2 (related to Figure 1). Clinical characteristics of Cohort 2-3.

Parameter	Bariatric surgery (n=21)				Never-obese (n=21)		Before bariatric surgery			After bariatric surgery		
	Before (A)	p-value (A vs. C)	After (B)	p-value (A vs. B)	Controls (C)	p-value (B vs. C)	Early onset (n=11)	Late onset (n=10)	p-value	Early onset (n=11)	Late onset (n=10)	p-value
Birth weight (g)							3540.2 ± 177.3	3420.0 ± 238.9	0.697			
Weight at 18 yr (kg)							81.3 ± 2.1	65 ± 2.7	0.000			
BMI at 18 yr (kg/m^2)							28.7 ± 0.8	22.6 ± 0.5	0.000			
Age (yr)	46.1 ± 2.1	0.621	48.0 ± 2.1	0.000	47.7 ± 2.2	0.608	43.0 ± 3.1	49.6 ± 2.5	0.118	44.6 ± 3.0	51.6 ± 2.4	0.092
BMI (kg/m^2)	41.1 ± 0.9	0.000	25.5 ± 0.6	0.000	25.1 ± 0.5	0.072	41.8 ± 1.4	40.4 ± 1.0	0.454	26.0 ± 0.5	24.9 ± 1.2	0.389
Waist (cm)	127.7 ± 1.9	0.000	87.8 ± 1.7	0.000	86.7 ± 1.5	0.432	126.8 ± 3.1	128.6 ± 2.3	0.654	87.4 ± 1.8	88.2 ± 3.2	0.818
Hip (cm)	128.9 ± 1.8	0.000	98.8 ± 1.5	0.000	99.6 ± 1.3	0.560	128.8 ± 2.5	129.1 ± 2.7	0.940	99.2 ± 1.5	98.3 ± 2.8	0.771
Waist-to-hip ratio	0.992 ± 0.012	0.000	0.891 ± 0.012	0.000	0.870 ± 0.012	0.054	0.985 ± 0.019	1.000 ± 0.014	0.528	0.887 ± 0.018	0.894 ± 0.017	0.795
Body fat (%)	52.8 ± 0.7	0.000	32.9 ± 1.5	0.000	34.6 ± 1.7	0.296	52.6 ± 1.0	53 ± 1.0	0.783	33.0 ± 1.0	32.8 ± 3.1	0.951
P-glucose (mmol/l)	5.6 ± 0.2	0.028	4.7 ± 0.1	0.000	5.1 ± 0.1	0.012	5.6 ± 0.3	5.6 ± 0.4	0.986	4.8 ± 0.2	4.6 ± 0.1	0.391
P-insulin (mU/l)	14.5 ± 2.0	0.000	4.2 ± 0.4	0.000	4.1 ± 0.4	0.921	13.0 ± 3.4	16.2 ± 2.1	0.449	3.9 ± 0.3	4.6 ± 0.7	0.406
Log_{10} $HOMA_{IR}$	0.5 ± 0.1	0.000	-0.1 ± 0.0	0.000	-0.1 ± 0.0	0.704	0.4 ± 0.1	0.6 ± 0.1	0.178	-0.1 ± 0.0	-0.1 ± 0.1	0.887
P-triglycerides (mmol/l)	1.7 ± 0.2	0.001	1.0 ± 0.1	0.000	0.9 ± 0.1	0.687	1.6 ± 0.2	1.9 ± 0.3	0.397	0.9 ± 0.1	1.0 ± 0.1	0.482
Average adipocyte volume (pl)	957.3 ± 44.9	0.000	369.4 ± 29.5	0.000	485.1 ± 35.5	0.005	959.8 ± 66.7	954.2 ± 62.1	0.953	346.1 ± 26.4	397.9 ± 57.9	0.398
Adipocyte number (10^{10} cells)	7.1 ± 0.4	0.006	7.6 ± 0.4	0.161	5.7 ± 0.3	0.002	6.9 ± 0.5	7.3 ± 0.6	0.646	7.5 ± 0.5	7.8 ± 0.8	0.759

Abbreviations: BMI, body mass index; $HOMA_{IR}$, homeostatic model assessment

Values are mean ± SEM

Table S4 (related to Figure 1). Pathways perturbed in obesity, but normalized by weight loss.

Resource	Pathway	Pathway ID	Adj. p-value
	DECREASED IN OBESITY, BUT INCREASED BY WEIGHT LOSS		
GO - biological process	Small Molecule Metabolic Process	GO:0044281	8.94E-06
GO - biological process	Carboxylic Acid Catabolic Process	GO:0046395	1.63E-05
GO - biological process	Organic Acid Catabolic Process	GO:0016054	1.63E-05
GO - biological process	Single-Organism Catabolic Process	GO:0044712	0.0002
GO - biological process	Small Molecule Catabolic Process	GO:0044282	0.0002
GO - biological process	Fatty Acid Metabolic Process	GO:0006631	0.0004
GO - biological process	Carboxylic Acid Metabolic Process	GO:0019752	0.0007
GO - biological process	Oxoacid Metabolic Process	GO:0043436	0.0013
GO - biological process	Organic Acid Metabolic Process	GO:0006082	0.0015
GO - biological process	Water-Soluble Vitamin Metabolic Process	GO:0006767	0.0026
GO - molecular function	Oxidoreductase Activity, Acting On Ch-Oh Group Of Donors	GO:0016614	0.0005
GO - molecular function	Oxidoreductase Activity, Acting On The Ch-Oh Group Of Donors, Nad Or N	GO:0016616	0.001
GO - molecular function	Alcohol Dehydrogenase (Nad) Activity	GO:0004022	0.003
GO - molecular function	Protein Dimerization Activity	GO:0046983	0.0047
GO - molecular function	Vitamin Binding	GO:0019842	0.0047
GO - molecular function	Anion Binding	GO:0043168	0.0047
GO - molecular function	Dipeptidase Activity	GO:0016805	0.0047
GO - molecular function	Cofactor Binding	GO:0048037	0.0047
GO - molecular function	Protein Homodimerization Activity	GO:0042803	0.0056
GO - molecular function	Amino Acid Binding	GO:0016597	0.0063
KEGG pathway	Insulin Signaling Pathway	4910	8.32E-05
KEGG pathway	Metabolic Pathways	1100	8.32E-05
KEGG pathway	Vitamin Digestion And Absorption	4977	0.0003
KEGG pathway	Nitrogen Metabolism	910	0.0003
KEGG pathway	Alanine, Aspartate And Glutamate Metabolism	250	0.0008
KEGG pathway	Tyrosine Metabolism	350	0.0017
KEGG pathway	Fatty Acid Metabolism	71	0.0017
KEGG pathway	Arginine And Proline Metabolism	330	0.0035
KEGG pathway	Glycine, Serine And Threonine Metabolism	260	0.006
KEGG pathway	Propanoate Metabolism	640	0.006
Wikipathways pathway	Adipogenesis	WP236	0.0003
Wikipathways pathway	Fatty Acid Biosynthesis	WP357	0.0006
Wikipathways pathway	Fatty Acid Omega Oxidation	WP206	0.0008
Wikipathways pathway	Ampk Signaling	WP1403	0.0008
	INCREASED IN OBESITY, BUT DECREASED BY WEIGHT LOSS		
GO - biological process	Immune System Process	GO:0002376	2.74E-46
GO - biological process	Immune Response	GO:0006955	2.88E-45
GO - biological process	Defense Response	GO:0006952	6.93E-39
GO - biological process	Inflammatory Response	GO:0006954	1.61E-26
GO - biological process	Response To Wounding	GO:0009611	1.06E-24
GO - biological process	Regulation Of Immune System Process	GO:0002682	8.22E-23
GO - biological process	Response To Stress	GO:0006950	2.26E-22
GO - biological process	Response To Stimulus	GO:0050896	1.25E-21
GO - biological process	Positive Regulation Of Immune System Process	GO:0002684	3.45E-21
GO - biological process	Regulation Of Immune Response	GO:0050776	3.07E-19
GO - cellular component	Cell Periphery	GO:0071944	3.73E-18
GO - cellular component	Plasma Membrane	GO:0005886	3.73E-18
GO - cellular component	Plasma Membrane Part	GO:0044459	1.09E-12
GO - cellular component	Membrane	GO:0016020	2.11E-12
GO - cellular component	Extracellular Space	GO:0005615	3.62E-12
GO - cellular component	Extracellular Region	GO:0005576	2.80E-11
GO - cellular component	Membrane Part	GO:0044425	2.80E-11
GO - cellular component	Extracellular Region Part	GO:0044421	6.01E-11
GO - cellular component	Intrinsic To Membrane	GO:0031224	2.36E-10
GO - cellular component	External Side Of Plasma Membrane	GO:0009897	1.17E-09
GO - molecular function	Igg Binding	GO:0019864	2.17E-11
GO - molecular function	Receptor Activity	GO:0004872	6.97E-10
GO - molecular function	Immunoglobulin Binding	GO:0019865	1.62E-08
GO - molecular function	Protein Complex Binding	GO:0032403	5.93E-06
GO - molecular function	Chemokine Activity	GO:0008009	1.73E-05
GO - molecular function	Receptor Binding	GO:0005102	1.73E-05
GO - molecular function	Chemokine Receptor Binding	GO:0042379	5.09E-05
GO - molecular function	Signaling Receptor Activity	GO:0038023	0.0006
GO - molecular function	Carbohydrate Derivative Binding	GO:0097367	0.0006
GO - molecular function	Signal Transducer Activity	GO:0004871	0.0006
KEGG pathway	Staphylococcus Aureus Infection	5150	3.45E-22
KEGG pathway	Phagosome	4145	5.86E-15
KEGG pathway	Osteoclast Differentiation	4380	5.86E-15
KEGG pathway	Leishmaniasis	5140	7.72E-10
KEGG pathway	Fc Gamma R-Mediated Phagocytosis	4666	8.98E-10
KEGG pathway	Systemic Lupus Erythematosus	5322	2.58E-09
KEGG pathway	Complement And Coagulation Cascades	4610	6.53E-09
KEGG pathway	Hematopoietic Cell Lineage	4640	6.73E-08
KEGG pathway	Chemokine Signaling Pathway	4062	1.78E-07
KEGG pathway	Natural Killer Cell Mediated Cytotoxicity	4650	3.43E-07
Wikipathways pathway	Complement And Coagulation Cascades	WP558	6.98E-07
Wikipathways pathway	Regulation Of Toll-Like Receptor Signaling Pathway	WP1449	2.90E-05
Wikipathways pathway	Focal Adhesion	WP306	8.40E-05
Wikipathways pathway	Complement Activation, Classical Pathway	WP545	8.40E-05
Wikipathways pathway	B Cell Receptor Signaling Pathway	WP23	0.0004
Wikipathways pathway	Toll-Like Receptor Signaling Pathway	WP75	0.0004
Wikipathways pathway	Inflammatory Response Pathway	WP453	0.0007
Wikipathways pathway	Osteoclast Signaling	WP12	0.0024
Wikipathways pathway	Il-3 Signaling Pathway	WP286	0.0048